JOURNAL OF PETROLOGY | VOLUME 38 | NUMBER 2 | PAGES 171–201 | 1997

The Geochemical Regimes of Piton de la Fournaise Volcano (Réunion) During the Last 530 000 Years

F. ALBARÈDE[1]*†, B. LUAIS[1]†, G. FITTON[2], M. SEMET[3]‡, E. KAMINSKI[1]†, B. G. J. UPTON[2], P. BACHÈLERY[4] AND J.-L. CHEMINÉE[3]‡

[1]LABORATOIRE DES SCIENCES DE LA TERRE, ECOLE NORMALE SUPÉRIEURE DE LYON, 46 ALLÉE D'ITALIE, 69364 LYON CEDEX 7, FRANCE

[2]DEPARTMENT OF GEOLOGY AND GEOPHYSICS, GRANT INSTITUTE, UNIVERSITY OF EDINBURGH, WEST MAINS ROAD, EDINBURGH EH9 3JW, UK

[3]INSTITUT DE PHYSIQUE DU GLOBE DE PARIS, 75252 PARIS CEDEX 05, FRANCE

[4]UNIVERSITÉ DE LA RÉUNION ET OBSERVATOIRE, 97418 LA PLAINE DES CAFFRES, RÉUNION

RECEIVED APRIL 30, 1996 REVISED TYPESCRIPT ACCEPTED SEPTEMBER 13, 1996

Piton de la Fournaise (Réunion, Indian Ocean) is a large active volcano which shares many features with the Hawaiian volcanoes. Its particularly simple elemental and isotopic geochemistry suggests, however, a rather homogeneous mantle source and makes this volcano ideally suited for petrogenetic studies. We report mineralogical descriptions, major element, trace element and Sr isotope compositions of four volcanic sequences spanning the 530 ka of the known lifetime of the volcano. The lavas change with time from mildly alkalic to mildly tholeiitic. This change is due to crystal fractionation becoming shallower with time as olivine replaces clinopyroxene as the liquidus phase at lower pressure. Fractionation of an olivine–clinopyroxene assemblage at lithospheric–mantle pressure drives tholeiitic basalts into the field of alkali basalts and puts some limitation on trace-element modelling of the melting process. Most Fournaise lavas are basalts with a narrow compositional range (steady-state basalts) and picrites containing common plastically deformed phenocrysts. The buffering of the compatible element compositions indicates that the lavas last equilibrated in solid-dominant conditions which are incompatible with magma chamber processes and may have resulted from the ascent of liquid-rich zones through dykes filled with a slurry of olivine ± clinopyroxene crystals. A quantitative model describing mass balance during the displacement of a solitary porosity wave leaving behind cumulates with residual porosity accounts for the major and trace element distributions. The dykes are flushed during major magma surges forming picritic slurries (= oceanites). The transient alkalic lavas are products of dynamic crystallization on cold dyke walls during times of lower magma fluxes. The total lifetime of a Réunion volcano (≥ 2·1 my) includes early and waning stages with alkalic activity bracketing a steady-state stage of tholeiitic activity. We estimate that Réunion volcanism results from the impingement on the base of lithosphere of a solitary wave of hotspot material with a radius of 100–130 km and a velocity of 5–9 cm/yr.

KEY WORDS: *Réunion; alkalinity; buffered differentiation; hotspot dynamics; assimilation*

INTRODUCTION

Most mature shield volcanoes from ocean islands erupt lavas with nearly constant compositions, and little understanding of the volcanic processes is to be expected from the repetitive analysis of nearly similar lavas. In contrast, the knowledge of the products emitted during the early and most variable stages of volcanic activity could potentially shed some light on how the melting regime and magma transfer through the oceanic lithosphere change while the plate carrying the volcanic edifice moves above

*Corresponding author.
†UMR CNRS 5570.
‡URA CNRS 1758.

the hotspot. The early studies of the waning stage in the life of a volcano (Macdonald & Katsura, 1964) and the discovery of a seamount representing a juvenile Hawaiian volcano at Loihi have identified a succession of volcanic regimes (Frey & Clague, 1983; Clague, 1987; Garcia *et al.*, 1995). Alkalic lavas both precede and follow the main tholeiitic stage of shield building. The dynamic causes of such a pattern are not yet entirely elucidated but both the extent of melting (Feigenson *et al.*, 1983) and interaction of plume-derived magmas with the lithosphere (Chen & Frey, 1983) are commonly perceived as major factors accounting for the dual character of ocean island volcanism.

Because of its long-standing isotopic homogeneity (McDougall & Compston, 1965; Fisk *et al.*, 1988), the Réunion hotspot is ideally suited for a geochemical investigation of the dynamics of volcanic processes associated with intraplate volcanoes. Piton de la Fournaise volcano has been active since at least 530 ka (Gillot *et al.*, 1990) and major source heterogeneity that can confuse petrogenetic modelling has been ruled out by the remarkable Sr and He isotopic homogeneity over the last 320 ka of its history (Graham *et al.*, 1990). Modern lavas are exclusively basaltic with a chemical composition transitional between tholeiitic and alkali basalts (Lacroix, 1936; Upton & Wadsworth, 1972*a*; Ludden, 1978; Clocchiatti *et al.*, 1979).

The present investigation is an attempt to assess both short-term and long-term variations in the geochemical dynamics of the volcano. The short-term variability of incompatible element ratios has been shown to be inconsistent with the presence of a large magma reservoir (Albarède, 1993; Albarède & Tamagnan, 1988) and supports short transfer times in agreement with the findings of U–Th–Ra disequilibria (Condomines *et al.*, 1988; Sigmarsson *et al.*, 1995). A new concept of 'buffered differentiation' will be offered as an explanation of the striking compositional homogeneity of most basaltic lavas. We report extensive mineralogical, major and trace element data, complemented by $^{87}Sr/^{86}Sr$ measurements, on both prehistoric and modern lavas. Particular emphasis will be placed on the interaction of lavas with older magmatic products (cannibalism). These data will be shown to constrain the evolution of the volcano and the rate of ascent of the parent hotspot material.

GEOLOGICAL OVERVIEW OF PITON DE LA FOURNAISE

Réunion (Fig. 1) is located in the Indian Ocean at 21°10′S, 55°30′W. Its position at the southern end of a well-defined hotspot track associates the Réunion volcanoes with the Deccan flood basalts whose eruption 65 my ago accompanied the separation of India from Gondwanaland (Duncan *et al.*, 1989). The age of the lithosphere under the island is 60 Ma (Bonneville *et al.*, 1988) and the absolute plate velocity above the hotspot is 0·15 deg/my or 1·7 cm/yr (Gripp & Gordon, 1990). The island, which is elongated in a northwest–southeast direction and forms an oval 50 km by 70 km, represents the aerial part of a much larger volcanic cone, 350 km in diameter (Lénat & Labazuy, 1990).

Réunion is composed of two large volcanic edifices, Piton des Neiges, to the northwest, and Piton de la Fournaise, to the southeast. Piton des Neiges has been active since at least 2·1 Ma (McDougall, 1971) and became extinct 10–20 ka ago (Deniel, 1990; Kieffer, 1990). The oldest lavas exposed on Piton de la Fournaise are found at the bottom of the deep canyons of Rivière des Remparts and Rivière de l'Est and have been dated at 527 ka (Gillot *et al.*, 1990). The volcano erupts, on average, once every 18 months. Stieltjes & Moutou (1989) reported a productivity of 0·01 km^3/yr (0·3 m^3/s) over the period 1931–1985.

The geology and the petrology of Piton de la Fournaise have been described in numerous papers. Recent activity is largely confined within a caldera ~8 km in diameter, open to the southwest as a result of gravitational collapse and known as l'Enclos. Radiocarbon dating suggests the caldera was formed 4745 yr ago (Bachèlery & Mairine, 1990). The mean elevation at the bottom western part of the caldera is relatively constant at ~2000 m. In the centre of l'Enclos, a cone rises to an altitude of ~2700 m. Two small craters (Dolomieu and Bory) formed at the top of the cone in the early 1930s. Rivers have deeply dissected the western part of the volcano and two prominent canyons (Rivière de l'Est and Rivière Langevin) appear to have been eroded along the fault bounding the old caldera which limits the Plaine des Sables to the west. The impressive canyon of Rivière des Remparts, west of Rivière Langevin, seems to utilize some old morpho-tectonic features (Bachèlery & Mairine, 1990). Some 150 ka ago, the volcanic centre moved eastward by 6–10 km from a position next to the Plaine des Sables to its present position. The seismic structure of the volcano has recently been investigated (A. Hirn, personal communication, 1995). A high-velocity plug 1·5 km in diameter underlies the Dolomieu crater down to sea-level and is rimmed by a low-velocity sheath which is thought to represent the outlet of the effusive products. No unambiguous seismic evidence of a magma reservoir was found.

The two Réunion volcanoes have strong petrological similarities (Lacroix, 1936; Upton & Wadsworth, 1966, 1972*a*; Ludden, 1978; Clocchiatti *et al.*, 1979; Nativel *et al.*, 1979; Albarède & Tamagnan, 1988; Fisk *et al.*, 1988; Sobolev & Nikogosian, 1994). The products of the two volcanoes are predominantly basalts, referred to as olivine, transitional or cotectic basalts, and hawaiites. For

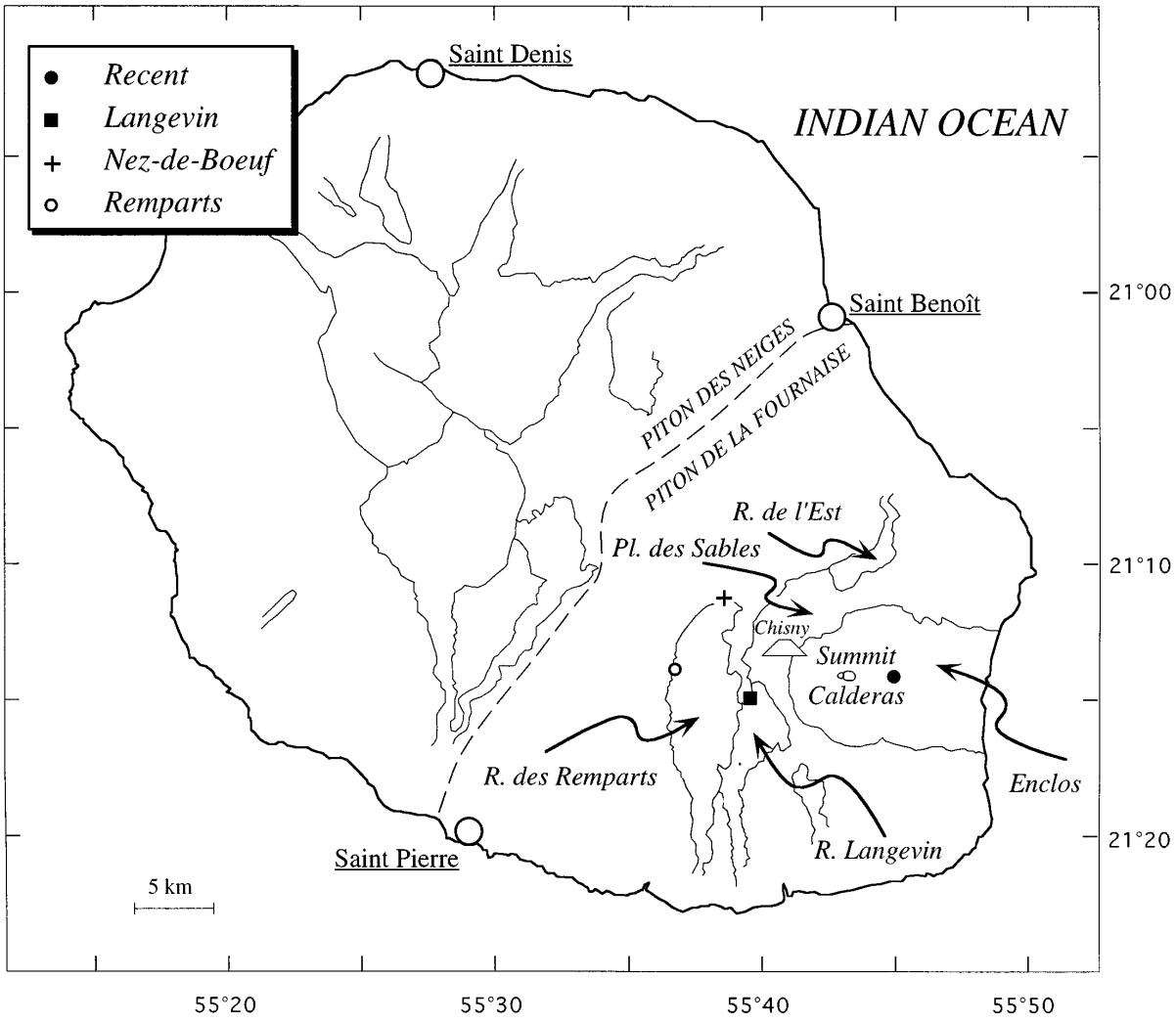

Fig. 1. Map of Réunion island. The now extinct Piton des Neiges volcano forms the northwestern part of the island and the active Piton de la Fournaise makes up the southeastern part. The major cliffs are outlined. Symbols indicate sampling sites.

the olivine-rich basalts, Lacroix coined the term 'oceanite', but, although we feel a need to discriminate MgO-rich melts from olivine-rich basalts, we will adhere to a more common usage and subsequently refer to these lavas as picritic basalts or, simply, picrites. Albarède & Tamagnan (1988) found evidence of up to three distinct phases of plastic deformation in picritic olivine, which they interpreted as xenocrysts. The waning stages of the Piton des Neiges abound in differentiated rocks, which were investigated in detail by Upton & Wadsworth (1972*a*) and Ludden (1978).

A recent account of the petrological diversity of the Piton de la Fournaise products has been given by Bachèlery & Mairine (1990). Making a distinction between an Old Shield and a Recent Shield, Ludden (1978) emphasized what turned out to be a remarkable period of volcanic quiescence. The K–Ar data of Gillot *et al.* (1990) dated that period between 290 and 220 ka whereas Bachèlery & Mairine (1990) described a deep canyon eroded in this interval at nearly the same location as the modern Rivière des Remparts and filled with ~100-ka-old lavas (Nez-de-Boeuf series). The oldest rocks, found in the Rivière des Remparts and Rivière de l'Est, are plagioclase-phyric basalts (Bachèlery & Mairine, 1990) and other differentiated lavas. Younger flows are almost exclusively olivine, picritic and occasional aphyric basalts. Fisk *et al.* (1988) presented some phase relationships for pressures up to 10 kbar in basalts and oceanites from the Piton des Neiges. Crystallization temperature determined from melt inclusion homogenization or chemical

thermometers (Sobolev *et al.*, 1983; Sobolev & Nikogosian, 1994; H. Bureau, personal communication, 1996) generally fall in the range 1160–1230°C.

Mantle xenoliths are absent. Babkine *et al.* (1966) and Upton & Wadsworth (1972*b*) described nodules of wehrlite and dunite cumulates from Piton de Chisny, a small cone 4 km west of the summit which last erupted in AD 800 (F. Albarède & M. Semet, unpublished radiocarbon dating). The cuttings recovered from the Grand Brûlé drill hole bored in the Remparts caldera at near sea-level indicated the presence of gabbros, wehrlite and dunite with traces of hydrothermal alteration at depths >1000 m (Augé *et al.*, 1989; Lerebour *et al.*, 1989; Rançon *et al.*, 1989).

Major and trace element modelling of Réunion lava compositions by Upton & Wadsworth (1972*a*), Ludden (1978) and Albarède & Tamagnan (1988) focused on fractional crystallization and partial melting. Albarède & Tamagnan (1988) showed that fractionation takes place below the plagioclase–clinopyroxene cross-over, i.e. at pressures >4 kbar, in disagreement with the concept of a shallow magma chamber inferred from seismic and magnetic observations. Melting of a source enriched in incompatible elements leaving a harzburgitic residue was a successful, although standard, result of inverting trace element melting equations.

SAMPLING AND FIELD OBSERVATIONS

Piton de la Fournaise commonly erupts alternating aa and pahoehoe lava flows. Depending on the local slope, the thickness of the flows varies from one to several metres, and they may extend downhill for several kilometres. Geochemical stratigraphy requires the knowledge of the time between two successive lava flows at the same site (mean return time). We measured the distribution of surface ages for historic lavas in the central and eastern part of l'Enclos, which is the closest to an active volcanic area offered by the modern Piton de la Fournaise. It was found that a lava surface may expect to survive 22 years (Fig. 2). This survival age translates into an accumulation rate of 45 m/ky for a typical flow thickness of 1 m. These figures apply only to the active area where lava flows are younger than 70 yr. Relatively inactive areas, such as the western part of l'Enclos, may remain uncovered for much longer times.

Sampling was designed (Fig. 1) to span most of the lifetime of the volcano:

(1) We first complemented the existing sampling of historical lava flows erupted from the early 1800s to 1986 with 23 samples taken from the less accessible east flank of the volcano (Grand Brûlé). The eruption dates are ascribed to flows with a variable degree of confidence,

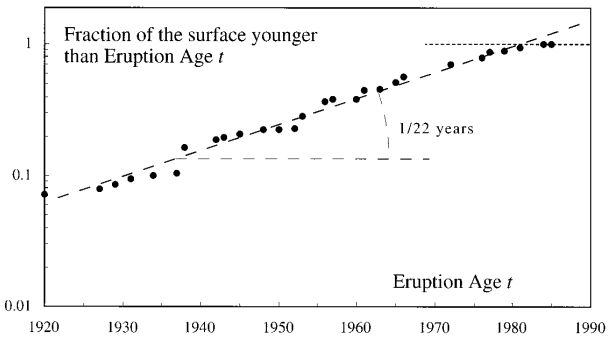

Fig. 2. Calculation of the return time between two lava flows at the same locality of l'Enclos caldera. The surface ages of the lava flows younger than 1920 obey an exponential distribution: the fraction F of lavas erupted at year t before the year $t_0 = 1986$ shown on the horizontal axis varies as $F = \exp(t - t_0)/\tau$, where τ is the return time. The linearity of this plot suggests that lava covers pre-existing flows at random (Poisson distribution). A lava flow is expected to remain exposed for 22 yr before it is covered by a younger flow.

based on old maps and interpretation of informal reports. In contrast to the older series, the elevations at which the samples were taken are not reported because of a broadly dispersed sampling, not necessarily carried out in vent areas. The modern samples tend to be compositionally bimodal. Basaltic samples with few to common (<10 vol. %) phenocrysts of clinopyroxene, olivine, Cr-spinel, and/or plagioclase contrast with picritic lavas with up to 50 vol. % of millimetre-sized olivine crystals. Occasionally, it is observed that the olivine crystals result from the disaggregation of olivine-rich cumulates. This is the case of the 1939 eruption at the Signal de l'Enclos, the 1977 lava flow of Piton Sainte Rose (see Fig. 4, below), and in the flows emitted from Piton de Chisny.

(2) Twenty-nine lava flows were cored by climbers from the series of the Morne Langevin cliff on the rim of the Rivière Langevin canyon at elevations of 1700–2200 m. The age of the top of the cliff is known to be 40 ka (Gillot *et al.*, 1990), and that of the bottom 70 ka (P.-Y. Gillot, personal communication). This series contains basalts and picrites, just as the younger series does. A few aphyric samples (LGV03, LGV07, LGV09) and one ankaramite sample (LGV14) were also recovered.

(3) The Nez-de-Boeuf lava series (1660–1850 m), thought to represent the volcanic infilling of an ancient canyon, was drilled for palaeomagnetic purposes by A. Chauvin. Two flows, sampled at 1840 and 1760 m, were dated at 105 and 180 ka, respectively, by P.-Y. Gillot. For a return time of the lavas of 22 years, such as observed in l'Enclos, the time span between the emplacement of the bottom and top lavas is equivalent to a few thousand flows. Very extended discontinuities must therefore be present within the series. Although the samples from this series were not inspected in as much detail as the other series, they appear to be olivine-bearing basalts.

(4) Thirty-two samples of the oldest series from the 700–1700 m western rim of the Rivière des Remparts canyon were cored by climbers. The oldest lavas in the canyon have been dated by K–Ar at 527 ka (Gillot *et al.*, 1990) whereas one lava flow sampled at 1390 m gave a K–Ar age of 395 ka (P.-Y. Gillot, unpublished data, 1991). The age of the flows at the top of the cliff (1700 m) is estimated, by interpolating the age of neighbouring samples, at 290 ka (Gillot *et al.*, 1990). Again, these ages are indicative of a very large proportion of stratigraphic hiatuses (>90% with reference to the eruption frequency in l'Enclos caldera). The bottom and the top of this series are very different. Above ~1300 m, the series is dominated by basaltic and picritic samples similar to those of recent eruptions. In the lower part, several samples (RP18, RP25, RP31, RP32) contain 30–50% plagioclase phenocrysts and occasional irregular clusters of plagioclase ± clinopyroxene crystals representing dismantled gabbroic fragments. Much more differentiated lavas, with compositions extending to mugearite and largely aphyric, are observed higher up in the series, most notably between 1150 and 1340 m (RP14, RP15, RP17, RP19, RP28).

ANALYTICAL TECHNIQUES

All the samples were examined in thin sections and then minerals were analysed with a Cameca SX-50 electron probe in Paris. The cores of lavas were rinsed in acetone and deionized water before crushing in an agate mortar. The whole rocks were analysed for major elements, and a selected set of trace elements in Edinburgh by X-ray fluorescence (XRF) according to the method described by Fitton *et al.* (1996) (see Table 2, below). A 100 mg aliquot of lava rock was dissolved in mixed HF–HNO_3–$HClO_4$ and analysed in Montpellier by inductively coupled plasma mass spectrometry (ICP-MS) according to the external calibration technique. The measurement of each series of 10 samples and one standard rock is preceded and followed by the analysis of a set of standard solutions. Interference corrections, reproducibility, precision, and data for standards have been reported by Albarède (1996). Accuracy with respect to the BE-N standard is generally better than 2% except for Th and U (4%). Typical 2σ reproducibility is 2–5% for most elements except for Yb, Lu, Th, U and Pb, for which it is 6–8%. A correction for blanks is routinely applied, which is invariably less than a few per cent. Isotopic spikes of Sr, Ba, Nd and Yb were added to the samples from the Rivière des Remparts series to monitor the sensitivity drift. Except for Nb, for which the solutions are unstable, overall excellent agreement was observed with the data obtained by XRF. For Sr isotopes, a 50–100 mg aliquot was dissolved in a similar mixture of acids and the solution evaporated to dryness. The samples were redissolved in HCl and Sr was separated on a strong cation-exchange resin upon elution by HCl and citric acid according to the method of Birck & Allègre (1978). The Sr fraction was loaded on an oxidized Ta filament and run on a double collector Micromass-30 in Clermont-Ferrand. The unweighted average $^{87}Sr/^{86}Sr$ value of the NBS 987 standard over the period when the present measurements were carried out is $0{\cdot}710207 \pm 24$. The entire chemical processing of the samples was carried out in Lyon.

MINERALOGY

Mean values of mineral compositions are given in Table 1. The Fe^{3+} contents have been calculated with the assumption of stoichiometric oxygen/cation proportions.

Olivine (97 microprobe analyses)

Cr-spinel inclusions are frequent and devitrified glass inclusions are common. Although rare phenocrysts may contain up to 89% forsterite, a strong frequency maximum is observed at 83–84% (Fig. 3), which corresponds to the literature descriptions and to the olivine composition in equilibrium with the FeO and MgO concentrations in common basalts. Iron-rich olivine is frequently observed as microphenocrysts. The CaO content of the olivine peaks at ~0·3% (Fig. 3), which is typical of basalt phenocrysts (Jurewicz & Watson, 1988a). Many olivine crystals seem to have a complicated history. Dislocations in olivine decorated by heating at 900°C for 1 h (Fig. 4a–c) following the technique of Kohlstedt *et al.* (1976) and mantled olivines (Fig. 4d) have been observed. As discussed below, no difference could be found in the chemistry of plastically deformed and undeformed crystals.

Clinopyroxene (101 analyses)

The pyroxenes are typical augites with Ca/(Ca + Fe + Mn + Mg) values of $0{\cdot}45 \pm 0{\cdot}01$. The chemical trends appear to reflect the extent of differentiation. In the Remparts series, high iron contents are associated with the most differentiated rocks. Principal component analysis (PCA) is a standard brute-force technique that extracts the direction of the most significant variations from a large data set with insufficient readability (e.g. Strang, 1988; Johnson & Winchern, 1992; Albarède, 1995). Some directions or components that are combinations of the initial variables account for a much larger fraction of the total variance than others and PCA provides an optimal selection of these directions. PCA amounts to the search of the eigenvalues and eigenvectors

Table 1: Average composition (with standard deviation given in parentheses) of the phenocrysts observed in the Piton de la Fournaise lavas

	Olivine	Clinopyroxene	Plagioclase	Spinel	Ti-magnetite 1	Ti-magnetite 2	Ilmenite
n	97	101	98	50	50	50	50
SiO_2	39·20 (0·52)	49·57 (0·95)	48·12 (1·56)	0·06 (0·02)	0·10 (0·05)	0·40 (0·83)	0·04 (0·04)
TiO_2	0·03 (0·01)	1·67 (0·44)	0·08 (0·04)	3·43 (0·73)	21·93 (3·20)	34·42 (1·07)	49·19 (1·11)
Al_2O_3	0·04 (0·05)	4·19 (0·65)	32·45 (0·90)	16·15 (0·70)	2·21 (1·51)	1·41 (0·61)	0·11 (0·08)
FeO	17·90 (2·28)	7·07 (0·84)	0·64 (0·06)	31·99 (0·84)	67·61 (2·25)	63·64 (1·56)	45·24 (0·53)
MnO	0·26 (0·05)	0·15 (0·06)	0·01 (0·02)	0·25 (0·06)	0·54 (0·13)	0·75 (0·08)	0·59 (0·16)
MgO	42·55 (1·96)	14·57 (0·65)	0·11 (0·03)	10·42 (0·30)	2·76 (1·33)	1·94 (0·43)	2·70 (1·00)
CaO	0·30 (0·04)	21·39 (0·66)	16·02 (1·08)	0·01 (0·01)	0·08 (0·12)	0·22 (0·26)	0·17 (0·07)
Na_2O	0·01 (0·02)	0·35 (0·07)	2·30 (0·76)	0·01 (0·01)	0·02 (0·01)	0·03 (0·02)	0·01 (0·01)
K_2O	0·01 (0·01)	0·01 (0·01)	0·10 (0·06)	0·00 (0·01)	0·01 (0·01)	0·02 (0·02)	0·02 (0·02)
NiO				0·21 (0·06)	0·03 (0·02)	0·07 (0·06)	0·03 (0·03)
Cr_2O_3				35·84 (0·80)	0·05 (0·03)	0·15 (0·11)	0·06 (0·06)
Total	100·30	98·97	99·83	98·37	95·34	103·05	98·16

of either the covariance matrix or the correlation matrix of the data. In the present case, no large variations in the analytical uncertainties on the data are expected and PCA has therefore been carried out on the correlation matrix [see Albarède (1995) for a discussion]. Calculation of components on the clinopyroxene correlation matrix shows that 62% of the variance is associated with one component which correlates negatively the group of Si and Mg with the group Ti, Al, ferric Fe, and Na. A second component accounting for 21% of the variance opposes ferrous Fe to Ca.

Plagioclase (98 analyses)

The maximum on the distribution of anorthite contents in the plagioclase phenocrysts from the Remparts series is at 84%. Phenocrysts from differentiated lavas and microphenocrysts are significantly more sodic (60–70%). Ferric iron enters the plagioclase molecule in the proportion of 0·025 atoms for 8 oxygens.

Oxides (50 analyses)

They are mostly Cr-spinel and Ti-magnetite with occasional ilmenite (Fig. 5). The composition of the Cr-spinel, frequently included in olivine phenocrysts, is rather constant with an average proportion of 45% chromite, 32% spinel and 21% magnetite components. The mean ratios $Cr/(Cr+Al) = 0{\cdot}593$, $Mg/(Mg+Fe^{2+}) = 0{\cdot}48$, $Fe^{3+}/(Fe^{3+}+Cr+Al) = 0{\cdot}14$, $Fe^{2+}/Fe^{3+} = 1{\cdot}9$ place the Réunion and Hawaii Cr-spinel in the same field, at oxygen fugacity about two orders of magnitude above the quartz–fayalite–magnetite (QFM) buffer (Horn *et al.*, 1994). Using the calibration of Fe^{2+}–Fe^{3+} equilibrium between spinel and liquid of Maurel & Maurel (1982), the average Fe^{2+}/Fe^{3+} ratio in the spinel indicates that $13 \pm 1\%$ of the iron in the basaltic liquid is ferric. The composition of the Ti-magnetite is clearly distinct from that of the Cr-spinel and much more variable. The occurrence of ilmenite is restricted to a few samples (LGV1, 16, RP1) and does not seem to be related to particular chemical characters.

Amphibole (3 analyses)

Only one crystal of hornblende was observed, in sample RP1.

GEOCHEMICAL RESULTS

Overview

As the large number of samples and elements analysed (Table 2) raises the suspicion that some major relationships may escape scrutiny through the reading of simple binary plots, we resorted once more to principal component analysis. The usual way of reporting PCA results is to plot the individual data points and the unit vector in the direction of each initial observation (e.g. Sr or Yb) in the component space with the unit circle being the trace of the 1σ ellipsoid. About 83·5% of the variability is accounted for by two components (Fig. 6). Each component of higher order accounts for 3·5% at most, which may not be significant. Many binary diagrams show an L-shaped spread of data: one arm of the L is made by the picritic basalts, the other by the

Table 2a: Major and trace element data

Sample:	R1301	O2201	R1201	Q1301	S1901	S1401	T1902	T2101	T1602	L2001	P1601	P1601	P1401	N2201	O2202	M1701	M1701O c	O1401	T1601	T1903	T1904	O1402	S1201
Date:	1700	1802	1905	1915	1920	1927	1927	1927	1931	1934	1939	1939	1942	1943	1943	1945	1945	1948	1952	1953	1953	1956	<1949
XRF																							
SiO_2	47·59	43·68	47·40	48·59	48·34	48·16	44·13	43·98	43·84	48·20	44·94	44·94	48·95	48·78	48·92	48·81	47·18	44·01	47·70	45·10	45·41	48·60	47·70
Al_2O_3	12·89	7·14	12·91	14·29	14·21	13·76	7·47	7·28	7·12	14·39	8·49	8·49	14·45	14·15	14·35	14·40	12·19	7·65	14·26	9·24	9·54	14·53	13·11
FeO	11·78	13·64	11·75	11·48	11·44	11·33	13·36	13·59	13·38	11·25	12·87	12·87	11·02	10·81	10·68	11·07	11·75	13·27	11·22	12·88	12·86	11·15	11·57
MgO	10·35	25·96	10·45	7·05	7·11	8·51	25·30	25·65	26·29	6·92	22·55	22·50	6·70	7·86	7·32	6·65	12·35	24·65	7·51	20·46	19·48	6·85	9·49
CaO	10·89	5·81	11·01	11·73	11·79	11·07	6·10	5·96	5·84	11·86	6·86	6·86	11·63	11·20	11·35	11·65	9·98	6·15	11·81	7·59	7·88	11·65	11·32
Na_2O	2·44	1·34	2·41	2·71	2·63	2·58	1·35	1·38	1·28	2·68	1·60	1·60	2·67	2·72	2·69	2·74	2·20	1·38	2·51	1·76	1·78	2·64	2·39
K_2O	0·71	0·39	0·78	0·80	0·76	0·81	0·38	0·37	0·36	0·78	0·44	0·44	0·76	0·79	0·78	0·79	0·65	0·41	0·78	0·51	0·54	0·79	0·76
TiO_2	2·43	1·35	2·57	2·71	2·73	2·68	1·36	1·33	1·28	2·75	1·63	1·63	2·69	2·78	2·80	2·68	2·36	1·46	2·77	1·78	1·85	2·74	2·59
MnO	0·18	0·20	0·18	0·18	0·17	0·17	0·19	0·19	0·19	0·17	0·19	0·19	0·17	0·17	0·16	0·17	0·18	0·20	0·17	0·19	0·18	0·17	0·18
P_2O_5	0·26	0·15	0·27	0·28	0·30	0·31	0·15	0·15	0·15	0·30	0·19	0·19	0·31	0·32	0·33	0·31	0·27	0·17	0·31	0·21	0·21	0·32	0·27
Sum	99·52	99·65	99·73	99·81	99·48	99·38	99·80	99·89	99·72	99·30	99·76	99·71	99·35	99·58	99·39	99·27	99·11	99·35	99·05	99·72	99·74	99·45	99·39
Nb	22·9	13·5	24·6	24·6	27·1	26·2	13·2	13·2	12·4	27·5	14·5	14·5	25·6	25·5	26·0	25·8	22·1	13·7	28·6	16·9	17·7	26·1	24·3
Zr	161·9	96·8	170·8	178·4	190·7	196·7	99·5	97·6	90·3	193·8	119·0	119·0	199·7	206·3	209·8	199·7	174·7	107·8	193·5	131·7	137·6	203·8	171·6
Y	25·5	14·5	25·3	28·0	28·9	29·0	14·6	14·7	13·0	28·5	17·5	17·5	29·0	30·1	30·3	29·1	25·8	15·6	27·8	18·5	19·8	29·2	26·6
Sr	322	183	345	353	361	363	185	181	173	364	214	214	370	373	374	368	314	192	364	241	251	371	342
Rb	18·6	10·0	20·1	19·7	19·6	20·6	9·5	9·3	9·2	20·6	11·3	11·3	19·8	19·2	19·5	20·0	16·1	10·1	21·3	13·3	14·0	21·0	19·4
Zn	106·2	107·4	101·1	100·1	106·3	101·7	107·1	106·2	103·3	104·7	107·3	107·3	104·1	99·0	97·7	107·4	109·0	110·3	104·8	105·2	106·9	105·8	103·4
Cu	109·4	61·4	105·1	110·0	109·8	101·2	66·3	60·1	58·0	108·3	66·7	66·7	110·6	103·5	104·2	108·7	122·0	72·7	121·2	70·6	74·1	109·7	108·5
Ni	249·5	1054·6	235·8	98·0	94·7	168·0	1012·8	1021·2	1041·7	85·9	850·4	850·4	83·7	143·2	112·5	86·5	354·3	976·2	120·8	767·2	716·0	96·5	202·5
Cr	592	1731	567	268	253	427	1712	1711	1687	229	1384	1384	211	393	332	217	769	1723	336	1358	1290	249	544
V	295·8	163·6	296·1	298·5	320·8	301·1	180·9	176·2	132·1	319·6	194·0	194·2	315·4	296·1	304·1	311·1	279·2	189·2	326·2	215·3	221·3	312·4	298·5
Ba	141·1	73·2	142·5	151·6	128·1	141·3	69·5	70·4	62·9	137·7	76·0	76·0	122·7	129·9	135·3	122·6	105·4	67·9	145·1	94·6	83·8	128·8	149·2
Sc	30·8	16·7	32·4	31·1	31·6	28·1	19·6	18·3	18·1	32·2	20·1	20·1	29·9	27·6	27·5	33·7	26·8	17·9	30·8	21·0	24·3	32·4	30·7

Table 2a: continued

Sample	R1301	O2201	R1201	Q1301	S1901	S1401	T1902	T2101	T1602	L2001	P1601	P1601	P1401	N2201	O2202	M1701	M1701O c	O1401	T1601	T1903	T1904	O1402	S1201
ICP-MS																							
Rb	16·6	10·0	14·6	11·8	17·3	17·4	8·80	8·80	8·10	19·2	8·40	11·9	20·9	19·1	20·0	18·5	15·7	10·0	13·1	11·0	11·2	19·7	16·1
Sr	307	177	311	307	337	343	175	171	161	332	198	224	375	348	364	337	293	185	314	220	229	347	316
Y	21·1	n.d.	19·8	21·6	23·4	23·7	11·6	11·3	10·5	n.d.	12·8	n.d.	n.d.	n.d.	n.d.	n.d.	n.d.	n.d.	21·3	14·5	15·1	n.d.	20·9
Nb	28·0	9·6	24·2	24·8	28·2	31·1	13·7	13·1	13·1	24·0	15·0	12·9	22·6	21·8	22·6	21·8	18·4	10·6	28·8	17·2	17·6	22·1	24·1
Cs	0·242	n.d.	0·503	0·160	0·255	0·256	0·132	0·138	0·124	n.d.	0·113	n.d.	n.d.	n.d.	n.d.	n.d.	n.d.	n.d.	0·189	0·160	0·166	n.d.	0·223
Ba	143·2	78·9	152·1	157·3	149·7	156·1	70·7	68·2	67·3	150·4	79·2	89·0	154·7	149·2	151·1	139·0	121·6	78·7	159·5	90·0	95·6	149·6	152·1
La	16·7	10·5	17·3	17·8	19·9	20·2	9·9	9·6	8·8	19·5	10·6	12·9	21·1	20·5	21·0	19·1	17·0	11·2	20·2	12·5	13·2	20·5	17·4
Ce	39·3	23·7	40·5	42·8	46·5	47·6	23·1	22·6	21·4	45·6	25·2	29·5	50·1	48·6	49·5	45·2	39·3	25·4	47·2	29·7	31·3	48·6	40·7
Pr	5·03	3·11	5·17	5·40	5·93	6·05	2·96	2·89	2·65	5·68	3·25	3·84	6·38	6·13	6·36	5·69	5·09	3·25	5·99	3·81	3·96	6·19	5·21
Nd	22·8	13·7	23·1	24·4	26·3	27·1	13·5	13·2	11·9	25·6	14·8	17·0	27·2	26·8	28·0	25·6	22·7	14·1	26·2	17·0	17·9	26·9	23·5
Sm	5·20	3·12	5·30	5·56	5·91	6·18	3·07	2·96	2·77	5·79	3·48	3·91	6·04	5·95	6·33	5·83	5·14	3·20	5·82	3·83	4·03	5·99	5·35
Eu	1·83	1·00	1·81	1·95	2·05	2·09	1·05	1·04	0·95	2·00	1·20	1·24	2·02	2·07	2·08	2·02	1·76	1·07	2·01	1·32	1·41	2·02	1·87
Gd	5·80	3·10	5·60	6·00	6·51	6·59	3·36	3·27	3·02	6·27	3·75	3·77	5·84	6·02	6·24	6·22	5·42	3·23	6·18	4·24	4·35	5·99	5·75
Tb	0·89	0·49	0·86	0·93	0·99	1·01	0·51	0·50	0·46	0·96	0·58	0·62	0·90	0·94	0·96	0·94	0·85	0·52	0·96	0·64	0·67	0·90	0·89
Dy	5·03	2·76	4·85	5·32	5·62	5·67	2·96	2·87	2·61	5·40	3·25	3·34	4·88	5·15	5·24	5·35	4·71	2·85	5·32	3·60	3·85	5·14	5·06
Ho	0·94	0·50	0·91	0·99	1·06	1·06	0·54	0·54	0·49	0·99	0·61	0·60	0·86	0·94	0·95	0·97	0·86	0·53	0·99	0·67	0·70	0·91	0·94
Er	2·42	1·38	2·28	2·48	2·66	2·69	1·36	1·33	1·23	2·60	1·48	1·66	2·36	2·47	2·54	2·55	2·24	1·39	2·45	1·67	1·76	2·48	2·38
Yb	1·97	1·12	1·83	2·04	2·13	2·10	1·10	1·08	0·97	2·22	1·16	1·33	1·97	2·16	2·15	2·21	1·91	1·22	1·98	1·35	1·41	2·10	1·94
Lu	0·30	0·17	0·28	0·31	0·32	0·32	0·17	0·16	0·15	0·33	0·18	0·20	0·28	0·31	0·30	0·31	0·29	0·18	0·29	0·20	0·22	0·30	0·29
Hf	4·81	2·34	4·81	5·09	5·34	5·69	2·55	2·71	2·53	4·32	3·28	2·89	4·03	4·50	4·46	4·58	4·07	2·56	5·22	3·60	3·76	4·33	4·86
Pb	1·87	1·12	1·86	2·43	2·10	2·16	1·15	1·04	2·34	2·55	1·06	1·40	2·21	2·04	2·14	2·19	1·71	1·71	2·31	1·22	1·44	2·18	1·67
Th	2·05	1·23	2·06	2·05	2·49	2·40	0·96	1·03	0·93	2·68	1·10	1·40	2·25	2·35	2·34	2·48	2·11	1·31	2·49	1·39	1·47	2·41	2·09
U	0·511	0·300	0·541	0·557	0·623	0·618	0·316	0·309	0·279	0·720	0·359	0·370	0·660	0·650	0·660	0·690	0·570	0·330	0·639	0·407	0·423	0·700	0·546
alk	–0·026	–0·003	0·086	–0·043	–0·071	0·003	–0·165	–0·091	–0·153	0·053	–0·157	–0·157	–0·248	–0·110	–0·197	–0·103	–0·173	–0·063	0·072	0·017	–0·055	–0·119	–0·066
Eu/Eu*	1·02	0·98	1·02	1·03	1·01	1·00	1·00	1·02	1·00	1·02	1·02	0·99	1·04	1·06	1·01	1·03	1·02	1·02	1·02	1·00	1·03	0·97	1·03
$^{87}Sr/^{86}Sr$	n.d.	n.d.	n.d.	n.d.	n.d.	n.d.	n.d.	n.d.	n.d.	n.d.	n.d.	n.d.	n.d.	n.d.	n.d.	n.d.	n.d.	n.d.	n.d.	n.d.	n.d.	n.d.	n.d.

Modern samples from l'Enlros. Alkalinity index = $(Na_2O + K_2O) - 0{\cdot}37(SiO_2–39)$. Eu* = $0{\cdot}327\sqrt{(Sm\ Gd)}$.

Table 2b: Major and trace element data

Sample:	LGV01	LGV02	LGV03	LGV04	LGV06	LGV07	LGV09	LGV12	LGV13	LGV14	LGV15	LGV16	LGV17	LGV18	LGV20	LGV21	LGV22	LGV23	LGV25	LGV26
Elev (m):	2300	2280	2260	2240	2200	2190	2160	2100	2080	2060	2040	1990	1980	1985	1960	1930	1910	1905	1870	1850
XRF																				
SiO_2	48·44	44·26	47·84	48·38	48·66	44·73	49·16	47·93	47·38	42·72	48·08	46·73	46·06	46·41	48·68	48·27	47·90	45·77	47·57	48·21
Al_2O_3	14·52	9·76	14·65	15·47	15·04	10·17	14·94	14·22	14·25	6·68	14·49	12·91	12·26	12·12	14·88	15·12	14·57	11·25	12·88	13·09
FeO	11·46	12·15	11·14	11·39	11·20	13·03	11·81	10·60	11·58	12·52	11·45	11·56	11·92	11·98	10·92	11·34	11·70	12·38	12·11	11·70
MgO	6·40	19·22	6·55	4·96	5·96	19·19	5·34	8·21	6·59	26·67	6·92	10·65	12·44	12·99	6·85	6·11	6·59	16·34	9·76	9·44
CaO	11·10	8·23	11·35	9·95	10·75	7·00	9·78	11·09	11·08	5·97	11·27	10·48	9·88	9·81	11·50	11·08	10·54	8·41	9·68	10·26
Na_2O	2·77	1·46	2·78	3·15	2·96	1·81	3·22	2·46	2·34	0·97	2·63	2·25	2·10	2·17	2·66	2·89	2·88	1·94	2·46	2·32
K_2O	0·69	0·43	0·89	0·98	0·90	0·53	0·98	0·61	0·55	0·22	0·72	0·81	0·77	0·77	0·74	0·91	0·92	0·60	0·73	0·53
TiO_2	2·68	1·78	2·92	3·20	2·99	1·88	3·17	2·49	2·60	1·20	2·61	2·53	2·44	2·44	2·65	3·04	3·01	1·92	2·88	2·41
MnO	0·17	0·18	0·16	0·17	0·17	0·18	0·18	0·17	0·17	0·18	0·18	0·18	0·17	0·18	0·17	0·17	0·18	0·18	0·18	0·18
P_2O_5	0·31	0·21	0·37	0·39	0·37	0·25	0·42	0·29	0·28	0·12	0·31	0·31	0·29	0·29	0·31	0·38	0·37	0·23	0·36	0·26
Sum	98·53	97·67	98·65	98·03	98·99	98·77	98·99	98·07	96·82	97·24	98·65	98·40	98·34	99·14	99·35	99·30	98·65	99·01	98·61	98·40
Nb	26·8	18·4	32·4	33·3	31·0	20·4	34·7	23·2	23·2	11·3	25·7	26·8	26·3	25·9	26·1	30·9	n.d.	19·8	27·4	23·8
Zr	202·9	138·5	238·0	253·0	240·5	152·0	266·8	186·4	180·1	82·2	195·6	187·4	178·7	177·9	194·4	234·8	n.d.	147·1	215·2	165·4
Y	28·9	17·5	28·6	33·7	32·1	19·8	36·2	25·9	28·3	11·9	28·1	25·4	22·9	23·3	27·4	29·3	n.d.	19·4	28·7	27·5
Sr	400	273	470	455	434	291	437	378	347	171	408	406	385	399	408	460	n.d.	308	361	317
Rb	15·1	7·3	21·0	22·7	21·2	10·6	20·7	13·4	12·3	3·9	17·4	20·8	20·0	20·0	14·9	18·8	n.d.	15·7	15·9	11·8
Zn	103·7	100·8	101·4	110·4	102·5	107·5	111·7	98·2	101·7	101·3	101·0	96·5	107·5	101·3	97·0	101·4	n.d.	103·8	104·3	107·9
Cu	82·3	84·8	70·4	56·0	78·9	56·0	79·4	89·1	90·0	65·2	103·4	93·7	91·4	73·3	108·5	79·2	n.d.	76·6	102·1	92·8
Ni	63·2	710·0	77·3	36·0	59·9	678·6	45·9	168·6	67·2	1165·2	88·0	266·1	369·3	380·2	96·3	63·8	n.d.	555·6	287·0	195·8
Cr	122	1271	151	54	119	1013	59	315	144	1697	162	561	714	689	174	55	n.d.	814	337	481
V	300·7	203·1	302·0	331·2	303·7	190·5	305·5	268·4	298·6	161·1	290·4	276·7	266·5	257·2	293·9	308·8	n.d.	217·2	294·7	262·8
Ba	158·6	124·3	206·9	218·0	192·5	130·2	201·7	144·2	145·5	74·0	166·6	191·9	181·5	185·2	167·1	197·4	n.d.	139·9	161·8	143·8
Sc	31·8	26·6	37·1	27·6	26·5	21·7	28·3	31·1	32·1	21·4	29·8	28·3	26·1	25·2	30·1	30·9	n.d.	25·2	29·2	27·1

Table 2b: continued

Sample:	LGV01	LGV02	LGV03	LGV04	LGV06	LGV07	LGV09	LGV12	LGV13	LGV14	LGV15	LGV16	LGV17	LGV18	LGV20	LGV21	LGV22	LGV23	LGV25	LGV26
Elev (m):	2300	2280	2260	2240	2200	2190	2160	2100	2080	2060	2040	1990	1980	1985	1960	1930	1910	1905	1870	1850
ICP-MS																				
Rb	13·0	6·69	19·3	21·3	20·1	10·1	19·7	12·2	11·8	3·66	15·8	18·1	19·1	18·9	14·4	18·4	21·5	14·6	15·4	12·1
Sr	358	253	441	429	408	278	408	335	329	160	376	391	373	369	399	455	422	293	353	314
Y	28·9	17·5	28·6	33·7	32·1	19·8	36·2	25·9	28·3	11·9	28·1	25·4	22·9	23·3	27·4	29·3	n.d.	19·4	28·7	27·5
Nb	24·2	17·0	30·8	31·1	28·9	19·2	32·4	20·3	19·2	8·9	20·7	23·6	22·9	21·7	22·0	26·9	26·9	16·6	23·5	20·3
Cs	0·182	0·089	0·113	0·290	0·180	0·121	0·232	0·195	0·188	0·066	0·272	0·282	0·209	0·296	0·132	0·098	0·100	0·097	0·259	0·223
Ba	144	107	189	206	184	117	205	123	133	60	156	179	168	161	156	194	192	129	152	138
La	20·5	14·5	25·5	25·8	23·9	16·3	27·2	17·5	18·2	8·7	19·9	21·7	20·5	19·8	20·5	25·4	25·3	15·6	23·1	19·5
Ce	47·7	34·2	58·9	59·6	55·9	37·4	62·5	41·1	43·5	20·7	47·0	50·7	48·0	45·9	47·9	58·8	57·2	35·8	52·5	42·8
Pr	6·07	4·41	7·30	7·50	7·11	4·71	7·86	5·26	5·57	2·66	6·03	6·35	6·05	5·78	6·08	7·45	7·36	4·67	6·77	5·43
Nd	26·9	19·4	31·7	32·9	31·2	20·7	34·4	23·5	25·2	12·0	26·7	28·1	26·4	25·1	27·0	32·9	32·1	20·4	30·0	23·9
Sm	6·21	4·28	6·97	7·37	7·19	4·65	7·82	5·42	6·08	2·81	6·29	6·23	5·96	5·64	6·25	7·38	7·25	4·74	6·80	5·62
Eu	2·15	1·44	2·37	2·51	2·44	1·55	2·65	1·88	2·07	0·95	2·14	2·08	1·99	1·89	2·13	2·50	2·38	1·55	2·23	1·94
Gd	6·39	4·60	7·04	7·57	7·37	4·82	8·16	5·70	6·34	2·92	6·40	6·22	5·90	5·67	6·41	7·36	7·39	4·93	7·16	6·44
Tb	1·01	0·65	1·06	1·15	1·14	0·73	1·24	0·87	1·01	0·46	1·00	0·94	0·89	0·86	0·98	1·12	1·10	0·74	1·08	0·99
Dy	5·67	3·59	5·74	6·41	6·32	4·10	7·00	4·86	5·80	2·60	5·64	5·31	4·99	4·82	5·54	6·25	6·08	4·12	6·00	5·68
Ho	1·03	0·65	1·03	1·18	1·16	0·74	1·28	0·88	1·07	0·48	1·03	0·96	0·91	0·88	1·00	1·12	1·13	0·76	1·13	1·08
Er	2·65	1·65	2·56	2·98	2·91	1·91	3·26	2·21	2·74	1·27	2·61	2·44	2·31	2·20	2·56	2·77	2·84	1·93	2·86	2·77
Yb	2·12	1·31	2·02	2·44	2·35	1·55	2·66	1·77	2·15	0·97	2·05	1·86	1·73	1·67	2·00	2·13	2·17	1·47	2·19	2·19
Lu	0·32	0·20	0·31	0·36	0·36	0·23	0·39	0·27	0·34	0·16	0·31	0·29	0·27	0·26	0·31	0·32	0·34	0·23	0·35	0·34
Hf	5·00	3·39	5·67	5·86	5·71	3·76	6·18	4·21	4·83	2·07	4·87	4·92	4·67	4·41	4·85	5·72	5·79	3·79	5·55	4·46
Pb	1·80	1·26	2·23	2·19	2·01	1·40	2·23	1·42	1·64	0·74	1·74	1·76	1·60	1·64	1·76	2·06	2·15	1·41	2·24	1·60
Th	2·60	1·74	3·28	3·24	2·87	1·94	3·31	2·05	2·39	0·73	2·51	2·68	2·56	2·45	2·55	3·07	3·33	2·02	2·93	2·63
U	0·667	0·473	0·870	0·832	0·771	0·508	0·857	0·529	0·603	0·274	0·648	0·678	0·670	0·591	0·629	0·756	0·817	0·509	0·719	0·601
alk	–0·034	–0·061	0·398	0·663	0·282	0·219	0·442	–0·229	–0·214	–0·188	–0·005	0·200	0·262	0·196	–0·181	0·371	0·507	0·032	0·020	–0·556
Eu/Eu*	1·04	0·99	1·03	1·03	1·02	1·00	1·01	1·03	1·02	1·01	1·03	1·02	1·03	1·02	1·03	1·04	0·99	1·02	0·98	0·99
$^{87}Sr/^{86}Sr$	0·704118	0·704161	0·704138	0·704101	0·704104	0·704103	0·704065	0·70409	0·70409	0·704211	0·704058	0·704209	0·704208	0·704227	0·704126	0·704119	0·704102	0·704163	0·704166	0·704042

Sample:	LGV27	LGV28	LGV29	R01	R02	R07	R03	R04	R05	R06	R08	R09	R10	R11	R12	R13	RP01	RP02	RP03	RP04
Elev (m):	1830	1820	1815	1850	1845	1800	1750	1730	1720	1710	1705	1695	1690	1675	1670	1665	1690	1670	1630	1605
XRF																				
SiO_2	47·68	47·45	45·84	47·55	47·11	47·58	46·79	47·24	47·27	47·72	48·43	47·83	48·51	45·95	46·59	47·05	47·27	44·69	47·52	47·43
Al_2O_3	14·14	13·48	11·01	14·52	14·17	13·46	13·92	14·56	13·96	14·35	15·83	15·68	16·08	13·59	14·17	13·74	13·97	9·23	14·22	14·40
FeO	11·39	11·45	13·76	11·41	12·05	12·11	12·29	12·31	11·39	11·39	11·28	11·27	11·09	12·01	11·98	12·20	12·25	13·16	12·97	13·12
MgO	7·12	10·37	16·03	6·89	9·96	9·17	9·28	9·14	8·77	8·20	6·34	6·23	5·79	10·35	9·83	10·28	8·04	21·11	7·00	6·90
CaO	10·97	10·34	8·33	11·31	8·60	9·41	9·62	8·88	10·15	10·05	9·10	9·10	8·90	10·13	9·17	9·31	11·21	8·07	9·82	10·03
Na_2O	2·44	2·48	1·98	2·82	2·99	2·73	2·70	2·93	2·60	2·88	3·36	3·23	3·48	2·40	2·80	2·77	2·52	1·51	3·15	2·97
K_2O	0·52	0·72	0·64	0·98	0·92	0·89	0·74	0·73	0·85	0·94	1·07	1·06	1·13	0·55	0·95	0·78	0·81	0·45	1·10	0·99
TiO_2	2·51	2·35	2·05	3·08	2·77	2·81	2·86	2·65	2·72	2·78	3·26	3·29	3·34	2·77	2·57	2·53	2·64	1·60	3·20	3·13
MnO	0·17	0·17	0·18	0·17	0·18	0·17	0·17	0·18	0·17	0·18	0·17	0·17	0·17	0·18	0·18	0·18	0·17	0·18	0·17	0·18
P_2O_5	0·28	0·28	0·26	0·38	0·39	0·39	0·34	0·35	0·36	0·37	0·43	0·43	0·45	0·34	0·36	0·33	0·38	0·22	0·49	0·43
Sum	97·22	99·08	100·07	99·12	99·13	98·71	98·71	98·97	98·23	98·85	99·27	98·29	98·94	98·26	98·60	99·17	99·26	100·21	99·64	99·58
Nb	22·2	24·7	21·4	31·9	30·9	31·0	25·4	25·1	28·6	28·9	35·2	35·1	37·6	27·7	29·4	26·5	27·3	14·9	36·6	34·3
Zr	182·1	176·0	157·9	234·5	234·9	234·4	220·9	217·4	216·3	220·7	258·4	258·5	274·6	217·8	214·7	199·2	202·4	119·9	269·8	252·5
Y	27·4	23·9	21·3	29·6	29·6	32·3	32·8	29·5	30·0	30·9	34·6	35·0	36·2	30·5	28·0	27·0	27·4	16·5	33·3	33·8
Sr	356	387	312	452	438	377	395	394	419	426	477	477	486	392	424	392	364	235	451	428
Rb	11·5	17·5	15·9	22·9	22·0	23·2	11·1	18·0	21·4	24·0	26·9	26·3	28·0	4·3	24·2	18·3	16·0	8·8	26·3	17·7
Zn	108·9	100·1	103·8	112·1	110·9	117·7	116·0	116·1	107·7	104·9	109·2	109·7	112·6	116·0	113·0	107·9	99·2	94·9	113·3	118·8
Cu	107·9	71·7	73·0	89·3	56·0	45·6	66·3	65·6	64·4	75·8	41·8	39·4	55·2	88·0	67·3	69·5	102·1	60·5	88·7	90·9
Ni	91·7	224·7	540·7	93·2	248·4	217·0	228·1	205·8	182·7	146·5	79·2	76·3	60·7	271·0	247·1	257·8	165·4	819·3	123·6	131·5
Cr	280	436	807	212	371	355	366	337	413	349	135	132	83	490	401	415	367	1449	192	195
V	273·9	252·7	203·3	317·4	244·6	282·5	261·4	241·2	278·3	277·5	291·9	288·6	309·9	291·1	272·0	250·5	272·7	164·8	280·6	274·9
Ba	131·3	174·6	156·1	204·9	191·5	170·3	145·9	146·2	192·4	196·4	221·3	226·1	222·6	165·6	200·0	166·1	115·3	71·5	155·8	144·1
Sc	26·6	24·2	22·5	33·5	22·2	26·2	26·2	22·4	27·0	27·2	21·5	21·6	21·3	29·3	26·1	22·9	35·7	26·4	21·3	30·0

Table 2b: continued

Sample:	LGV27	LGV28	LGV29	R01	R02	R07	R03	R04	R05	R06	R08	R09	R10	R11	R12	R13	RP01	RP02	RP03	RP04
ICP-MS																				
Rb	10·5	15·8	15·2	21·0	16·0	19·4	10·2	14·8	20·4	17·8	25·9	24·5	24·9	4·69	20·4	16·7	16·9	9·23	27·1	18·5
Sr	334	363	292	435	384	352	370	363	401	389	459	457	456	373	389	368	366	228	442	427
Y	27·4	23·9	21·3	24·6	22·5	25·4	25·9	23·3	24·8	23·9	29·0	29·0	29·2	25·0	22·4	22·4		17.2	32·5	33·5
Nb	17·6	20·6	18·3	32·8	31·2	31·3	25·4	24·9	32·0	29·8	34·9	34·7	36·8	28·0	28·2	26·4	37·3	17·8	46·5	32·7
Cs	0·178	0·142	0·098	0·220	0·104	0·214	0·068	0·198	0·188	0·143	0·167	0·186	0·166	0·055	0·104	0·341	0·185	0·083	0·160	0·073
Ba	123	158	141	196	174	165	148	141	184	184	217	215	221	162	196	150	167	91	219	211
La	17·7	19·2	17·3	23·4	23·6	23·3	19·8	20·3	21·7	21·9	26·3	26·3	27·2	20·8	21·3	20·7	21·1	11·3	26·5	25·1
Ce	41·2	43·9	39·2	54·3	54·1	53·9	46·8	47·7	49·8	50·5	60·9	60·2	62·2	48·3	49·4	47·5	49·3	26·8	61·8	59·4
Pr	5·55	5·66	5·13	6·99	6·78	6·94	6·12	6·27	6·43	6·50	7·72	7·68	7·87	6·22	6·16	6·01	6·45	3·57	8·04	7·68
Nd	24·6	25·1	22·3	31·4	29·7	30·8	27·9	28·1	28·6	29·0	34·2	34·1	34·8	28·0	27·8	26·7	27·8	15·7	34·2	32·9
Sm	5·87	5·72	5·04	7·02	6·48	7·02	6·58	6·48	6·44	6·55	7·63	7·60	7·81	6·34	6·00	5·85	6·16	3·64	7·51	7·33
Eu	2·00	1·95	1·74	2·35	2·21	2·31	2·25	2·20	2·22	2·24	2·61	2·58	2·67	2·21	2·10	2·06	2·09	1·23	2·44	2·39
Gd	6·36	6·40	5·23	7·07	6·69	7·31	7·07	6·67	6·87	6·88	8·06	7·93	8·17	6·92	6·41	6·32	6·28	3·78	7·43	7·25
Tb	0·96	0·90	2·69	1·08	1·00	1·11	1·08	1·02	1·04	1·05	1·21	1·21	1·26	1·06	0·96	0·96	1·01	0·60	1·11	1·12
Dy	5·46	5·02	4·46	5·92	5·56	6·23	6·17	5·67	5·89	5·81	6·76	6·80	6·93	5·91	5·34	5·41	5·44	3·29	6·25	6·25
Ho	1·01	0·93	0·80	1·08	1·01	1·13	1·13	1·04	1·10	1·08	1·26	1·25	1·29	1·10	0·99	1·00	1·06	0·62	1·16	1·16
Er	2·59	2·36	1·98	2·69	2·58	2·84	2·89	2·60	2·78	2·72	3·20	3·19	3·23	2·75	2·48	2·45	2·67	1·58	3·00	3·04
Yb	2·00	1·77	1·61	2·11	2·03	2·28	2·34	2·07	2·27	2·22	2·57	2·59	2·60	2·22	2·03	1·96	2·22	1·35	2·46	2·48
Lu	0·31	0·27	0·24	0·31	0·31	0·34	0·34	0·31	0·34	0·33	0·39	0·39	0·40	0·33	0·30	0·30	0·38	0·22	0·36	0·36
Hf	4·67	4·56	4·19	6·89	6·38	6·52	6·03	5·94	6·07	6·09	7·12	7·10	7·28	5·79	5·61	5·39	5·59	3·30	6·42	5·97
Pb	1·54	1·79	1·50	2·34	1·89	1·81	1·81	1·69	2·07	1·98	2·18	2·42	2·25	1·89	2·02	1·77	n.d.	n.d.	n.d.	n.d.
Th	2·16	2·43	2·17	2·96	2·86	2·82	2·39	2·35	2·70	2·56	3·31	3·27	3·45	2·61	2·65	2·62	3·13	1·60	3·46	3·32
U	0·526	0·332	0·574	0·714	0·671	0·730	0·540	0·650	0·690	0·689	0·827	0·827	0·883	0·652	0·658	0·621	0·804	0·432	0·940	0·449
alk	–0·246	0·075	0·086	0·637	0·904	0·444	0·560	0·612	0·385	0·594	0·942	1·024	1·094	0·375	0·944	0·570	0·266	–0·146	1·095	0·843
Eu/Eu*	1·00	0·99	1·04	1·02	1·03	0·99	1·01	1·02	1·02	1·02	1·02	1·02	1·02	1·02	1·04	1·04	0·97	0·99	1·00	1·00
$^{87}Sr/^{86}Sr$	0·704047	0·704091	0·704106	n.d.	n.d.	n.d.	n.d.	n.d.	n.d.	n.d.	n.d.	n.d.	n.d.	n.d.	n.d.	n.d.	0·704179	0·704122	0·704136	0·704083

Sample:	RP05	RP06	RP07	RP09	RP10	RP11	RP12	RP13	RP14	RP15	RP16	RP17	RP18	RP19	RP20	RP21	RP23	RP24	RP25	RP26
Elev.(m):	1590	1550	1540	1390	1370	1345	1330	1280	1270	1240	1200	1190	1170	1145	1110	1080	990	910	890	850
XRF																				
SiO_2	47·10	47·58	47·78	47·30	47·62	45·78	45·31	47·01	47·93	52·91	47·02	48·17	46·55	52·16	46·81	47·13	45·81	47·25	46·79	46·22
Al_2O_3	14·66	15·10	15·16	15·28	14·21	12·91	13·83	15·15	16·04	15·99	15·04	15·01	17·05	15·81	15·29	14·86	14·38	14·24	19·28	14·80
FeO	13·22	12·16	11·79	12·35	13·12	13·65	14·26	14·48	12·84	10·10	12·98	13·85	11·20	10·28	12·54	12·79	15·07	14·54	10·96	14·10
MgO	6·46	6·23	7·01	6·19	7·03	10·96	10·16	4·77	4·29	3·04	7·50	4·10	6·08	3·34	7·07	6·55	4·89	5·84	3·65	5·21
CaO	11·65	11·20	10·74	11·37	10·39	10·52	9·39	9·30	9·48	6·41	10·29	8·36	11·66	7·05	11·50	11·73	9·70	11·01	11·23	10·06
Na_2O	2·60	2·77	2·94	2·77	2·86	2·28	2·56	3·54	3·70	5·04	2·83	3·87	2·71	4·67	2·33	2·59	3·06	2·86	2·82	3·19
K_2O	0·72	0·91	0·97	0·92	0·91	0·65	0·96	1·31	1·30	2·36	0·85	1·47	1·11	2·10	0·68	0·72	0·92	0·75	0·73	0·88
TiO_2	2·85	3·01	2·81	2·84	3·05	2·49	2·74	3·41	3·35	2·50	2·90	3·50	2·60	2·76	2·63	2·56	3·70	3·03	2·70	3·13
MnO	0·18	0·17	0·17	0·17	0·18	0·18	0·18	0·20	0·18	0·19	0·17	0·19	0·16	0·19	0·17	0·18	0·20	0·18	0·15	0·19
P_2O_5	0·37	0·39	0·37	0·34	0·37	0·35	0·38	0·48	0·57	0·92	0·36	0·57	0·40	0·84	0·30	0·29	0·47	0·32	0·34	0·44
Sum	99·80	99·52	99·74	99·53	99·73	99·77	99·77	99·64	99·68	99·46	99·94	99·09	99·52	99·20	99·32	99·40	98·21	100·02	98·65	98·22
Nb	27·9	31·4	30·4	28·9	28·4	21·8	31·7	39·5	41·6	72·7	28·7	48·6	35·6	58·4	25·3	23·4	31·6	25·1	24·0	35·9
Zr	212·9	238·1	211·8	207·8	224·0	159·9	218·1	269·2	268·8	493·1	211·4	327·4	222·8	407·5	181·7	176·9	210·6	183·0	163·3	236·6
Y	29·3	30·6	29·4	27·7	31·9	24·0	26·4	34·7	36·6	57·8	30·4	42·7	25·9	48·7	25·4	25·2	30·5	28·4	21·7	32·8
Sr	414	444	432	432	405	348	436	461	494	448	409	463	539	417	399	391	441	419	540	445
Rb	10·7	20·0	23·3	22·5	20·8	15·0	19·6	33·7	32·1	59·7	14·4	38·0	27·7	53·9	16·6	15·7	22·7	18·4	17·3	16·5
Zn	106·9	106·6	100·4	103·2	105·6	106·0	114·8	122·5	113·0	128·3	110·6	125·4	89·3	124·7	101·8	108·4	117·9	113·2	87·7	123·5
Cu	118·9	128·8	62·7	95·7	86·8	73·6	70·1	61·4	28·9	11·4	54·6	25·9	84·6	14·3	71·8	105·2	95·9	72·3	66·0	83·9
Ni	69·9	84·4	109·4	83·4	118·4	230·9	220·2	23·9	15·3	2·1	109·2	6·9	84·3	2·2	98·5	74·6	35·1	35·0	29·1	36·0
Cr	74	129	284	132	206	543	420	18	22	-1	170	14	200	3	302	82	50	39	41	30
V	295·3	277·8	273·6	271·2	264·4	263·4	239·3	334·2	268·6	95·3	284·4	256·4	256·6	135·1	221·9	299·7	339·2	329·3	244·8	238·7
Ba	116·8	124·7	156·9	135·2	122·3	87·4	164·0	206·5	228·7	430·2	121·8	251·1	204·1	369·8	126·7	111·8	144·6	98·7	112·5	183·3
Sc	36·6	32·0	28·3	31·0	32·4	34·7	23·9	22·2	26·5	13·2	29·8	23·3	23·6	7·5	35·6	37·6	33·1	37·3	23·4	29·3
ICP-MS																				
Rb	11·6	20·5	24·5	23·0	21·8	16·1	20·4	34·6	33·4	61·3	15·0	38·2	28·6	58·6	17·5	16·0	23·3	19·0	17·9	17·3
Sr	411	443	431	434	407	358	445	471	493	456	414	468	550	452	407	394	442	422	545	458
Y	28·9	30·7	28·8	28·5	31·8	24·7	26·6	34·7	35·4	55·8	30·3	41·5	25·6	50·2	26·6	25·1	30·1	28·1	22·6	33·0
Nb	38·4	35·1	37·8	34·8	32·8	27·3	39·8	48·2	52·9	86·5	38·8	63·2	49·9	81·5	36·2	30·6	41·0	32·4	33·5	46·5
Cs	0·244	0·113	0·167	0·420	0·250	0·250	0·160	0·380	0·200	0·360	0·218	0·236	0·316	0·664	0·320	0·163	0·200	0·144	0·332	0·264
Ba	176	185	205	198	181	141	224	274	299	510	179	321	257	430	173	156	221	173	179	251
La	21·1	23·6	22·9	21·7	23·0	16·3	23·6	30·0	30·7	56·3	21·9	36·6	25·5	45·2	18·5	17·7	22·3	18·6	17·1	26·6
Ce	50·2	55·3	52·7	50·0	51·7	38·4	53·4	67·7	70·0	125·9	50·9	81·6	57·6	103·1	42·6	41·3	52·1	42·7	41·3	59·4
Pr	6·61	7·23	6·87	6·67	6·88	5·16	6·96	8·68	8·95	15·71	6·75	10·66	7·21	13·05	5·69	5·40	6·84	5·70	5·39	7·78
Nd	28·6	31·5	29·8	28·6	30·3	23·1	29·6	36·8	38·1	65·1	29·6	45·4	30·5	55·3	24·7	23·9	30·2	25·6	23·2	33·6
Sm	6·54	6·91	6·60	6·35	6·81	5·27	6·34	7·83	8·15	13·29	6·69	9·57	6·36	11·69	5·69	5·40	6·78	5·90	5·11	7·10
Eu	2·20	2·30	2·18	2·23	2·30	1·85	2·08	2·53	2·72	4·15	2·25	3·05	2·10	3·66	2·01	1·86	2·35	2·06	1·94	2·38
Gd	6·65	6·98	6·74	6·41	6·99	5·45	5·97	7·48	7·89	12·67	6·29	8·92	5·69	10·98	5·64	5·27	6·40	5·74	5·08	6·79
Tb	1·06	1·05	1·03	1·06	1·08	0·83	0·90	1·13	1·17	1·92	1·06	1·38	0·86	1·67	0·97	0·85	0·99	0·91	0·88	1·05
Dy	5·71	5·90	5·75	5·49	5·95	4·67	5·09	6·45	6·74	10·88	5·80	7·77	4·92	9·44	5·17	4·79	5·69	5·26	4·44	6·07
Ho	1·12	1·11	1·05	1·11	1·13	0·86	0·91	1·17	1·23	2·03	1·13	1·44	0·89	1·73	1·04	0·88	1·03	0·96	0·91	1·14
Er	2·79	2·83	2·74	2·70	2·88	2·20	2·40	3·14	3·34	5·48	2·87	3·85	2·36	4·72	2·62	2·34	2·73	2·58	2·21	2·99
Yb	2·32	2·36	2·24	2·24	2·35	1·82	1·89	2·54	2·67	4·36	2·34	3·14	1·92	3·80	2·13	1·91	2·20	2·11	1·81	2·49
Lu	0·39	0·35	0·33	0·42	0·35	0·27	0·27	0·37	0·39	0·63	0·41	0·45	0·27	0·55	0·41	0·29	0·31	0·30	0·40	0·38
Hf	5·88	5·91	5·61	5·24	5·60	4·26	5·99	6·99	7·08	11·72	6·19	8·29	6·09	9·88	5·45	5·22	5·77	5·31	5·06	6·70
Pb	n.d.	n.d.	n.d.	1·17	1·93	1·43	2·36	2·66	2·46	4·85	2·49	3·07	2·54	3·98	1·64	1·71	1·99	2·57	2·02	2·52
Th	2·95	3·26	2·85	2·74	2·76	2·11	2·89	3·69	3·68	7·50	2·83	4·50	3·35	5·57	2·42	2·23	2·76	2·38	2·34	3·71
U	0·683	0·870	0·761	0·790	0·770	0·570	0·760	1·010	0·920	1·530	0·485	1·109	0·813	1·453	0·600	0·540	0·658	0·592	0·688	0·700
alk	0·321	0·501	0·662	0·620	0·576	0·417	1·181	1·883	1·693	2·254	0·716	1·948	1·026	1·899	0·120	0·305	1·464	0·557	0·670	1·396
Eu/Eu*	0·98	0·99	1·00	0·94	0·98	0·95	0·97	0·99	0·96	1·02	0·94	0·99	0·94	1·01	0·92	0·94	0·91	0·92	0·86	0·95
$^{87}Sr/^{86}Sr$	0·704148	0·704148	0·704092	0·704137	0·704118	0·704114	0·704053	0·704145	0·704061	0·704084	0·704149	0·704056	0·704156	0·70405	0·704104	0·704115	0·704063	0·704049	0·704034	0·704093

Table 2b: continued

Sample:	RP27	RP28	RP29	RP30	RP31	RP32	Steady-state
Elev (m):	810	790	760	750	740	720	
XRF							
SiO_2	47·70	49·07	47·36	46·60	47·04	46·05	47·6
Al_2O_3	14·95	14·80	14·18	14·38	16·67	17·27	14·6
FeO	13·48	12·89	15·36	14·51	11·71	12·94	12·1
MgO	5·16	4·08	5·05	5·46	5·27	4·62	7·1
CaO	10·45	8·20	10·07	9·62	11·79	11·16	10·6
Na_2O	3·04	4·01	3·19	3·02	2·67	2·78	2·8
K_2O	0·92	1·48	0·84	1·03	0·53	0·73	0·8
TiO_2	3·06	3·35	3·37	3·37	2·52	2·92	2·9
MnO	0·18	0·19	0·21	0·19	0·16	0·19	0·2
P_2O_5	0·48	0·81	0·48	0·48	0·37	0·34	0·4
Sum	99·42	98·89	100·11	98·65	98·72	98·99	
Nb	31·7	52·0	30·8	32·2	20·0	21·9	28·9
Zr	201·8	298·7	228·9	221·2	147·8	148·6	214
Y	30·5	40·3	36·4	31·4	23·1	23·4	29·8
Sr	450	497	429	403	462	458	414
Rb	25·9	38·7	12·6	25·3	6·9	12·9	19·1
Zn	112·6	120·4	124·8	115·6	88·9	94·4	107
Cu	65·0	18·5	90·4	73·8	66·5	51·9	84
Ni	36·2	3·3	24·4	33·4	37·2	23·5	114
Cr	53	5	19	34	46	32	216
V	313·5	198·8	350·8	344·9	280·6	322·2	288
Ba	157·3	261·5	127·3	140·6	98·4	107·0	159
Sc	28·6	21·0	33·7	32·1	24·1	25·9	29·3
ICP-MS							
Rb	26·6	39·5	13·6	25·3	7·6	14·7	17·9
Sr	456	506	438	402	473	483	399
Y	30·5	39·5	35·9	31·5	23·8	24·6	27·6
Nb	41·5	66·4	44·1	41·9	26·5	30·1	31·5
Cs	0·440	0·277	0·416	0·320	0·166	0·276	0·2
Ba	217	328	212	199	142	165	179
La	23·7	37·0	27·6	23·4	16·8	17·3	22·1
Ce	54·2	84·3	57·6	54·9	39·9	40·6	51·0
Pr	7·03	10·62	8·16	7·19	5·30	5·42	6·6
Nd	30·8	45·5	35·2	31·5	23·7	23·8	29·0
Sm	6·61	9·18	7·59	6·78	5·16	5·33	6·5
Eu	2·30	3·05	2·66	2·29	1·83	1·92	2·2
Gd	6·34	8·81	7·38	6·65	4·94	5·18	6·7
Tb	0·97	1·29	1·23	1·01	0·75	0·84	1·03
Dy	5·66	7·34	6·70	5·90	4·51	4·74	5·8
Ho	1·04	1·36	1·31	1·09	0·83	0·90	1·07
Er	2·74	3·56	3·34	2·87	2·15	2·35	2·7
Yb	2·27	2·87	2·75	2·34	1·76	1·90	2·2
Lu	0·33	0·43	0·50	0·35	0·27	0·32	0·34
Hf	5·86	7·67	6·62	6·28	4·62	4·90	5·7
Pb	2·24	2·79	2·50	2·08	1·50	1·80	
Th	3·14	4·98	3·26	3·03	1·95	2·25	2·8
U	0·729	1·091	0·764	0·718	0·402	0·320	0·684
alk	0·739	1·766	0·941	1·237	0·229	0·900	0·44
Eu/Eu*	0·92	0·96	0·92	0·96	0·90	0·89	1·03
$^{87}Sr/^{86}Sr$	0·704074	0·704086	0·704129	0·704123	0·704117	0·704065	

Sample provenance: RPXX, Remparts; RXX, Nez-de-Bœuf; LGVXX, Langevin. Alkalinity index = $(Na_2O + K_2O) - 0{\cdot}37(SiO_2 - 39)$. Eu* = $0{\cdot}327\sqrt{(Sm\ Gd)}$. Steady-state: mean value of basalts with 5% < MgO < 10%.

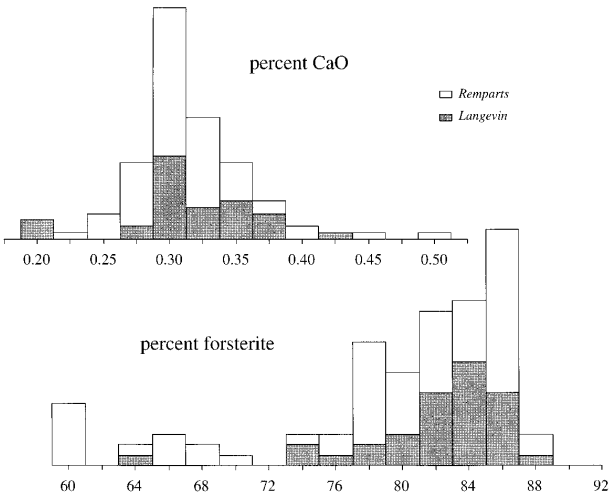

Fig. 3. Olivine compositions: histograms of forsterite (bottom) and CaO (top) contents. The smallest rectangles correspond to one measurement.

differentiated lava flows from the Remparts series. The common basalts cluster at the apex. This pattern is

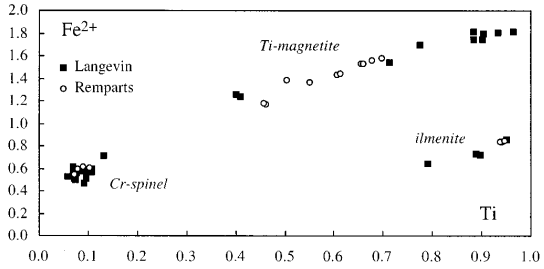

Fig. 5. The three oxide phases present in the Piton de la Fournaise lavas in a Fe^{2+} vs Ti plot.

extremely similar to that described for the Mauna Loa lava compositions by Rhodes (1988).

Major elements

The mean value and standard deviation of selected concentrations and elemental ratios in the whole-rock samples are given in Table 3. For many of these parameters, a smooth pattern of temporal evolution is

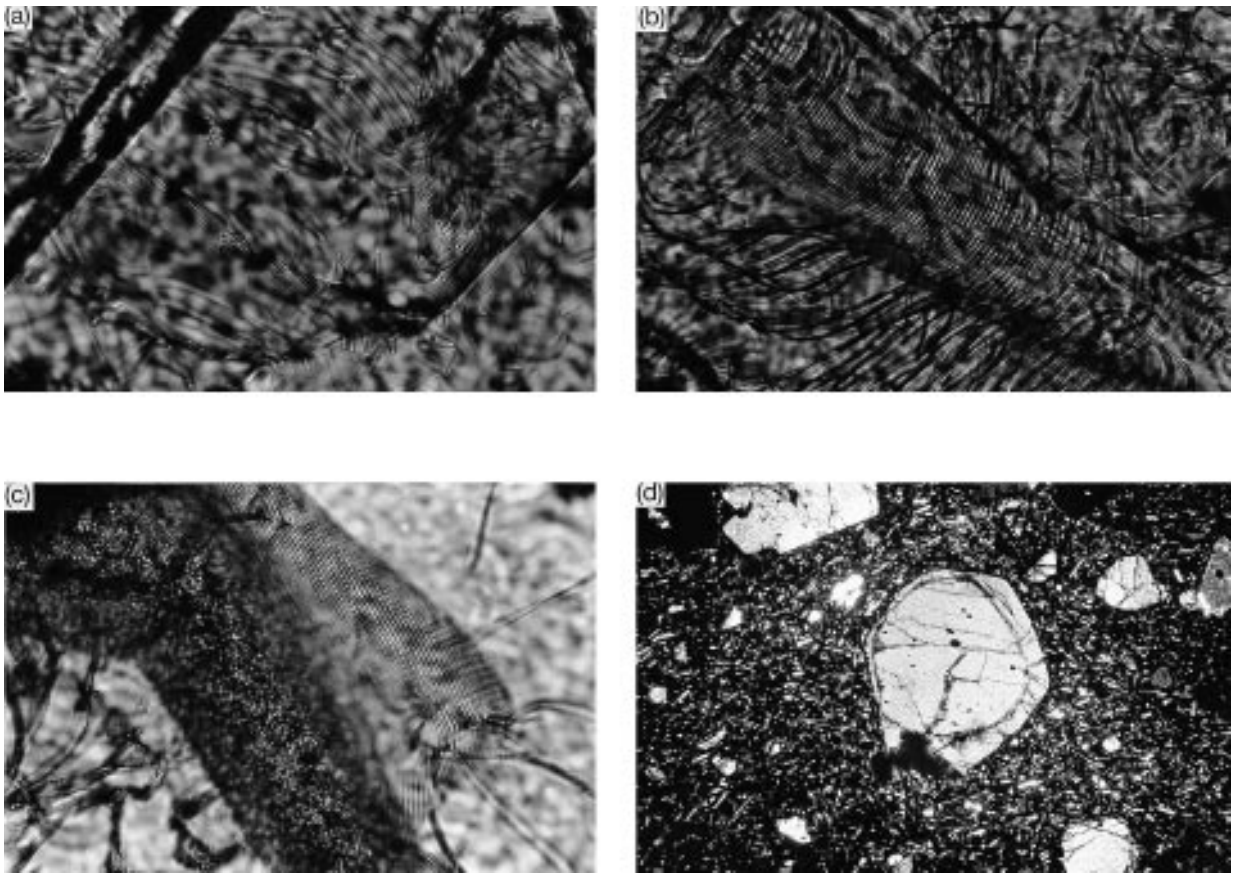

Fig. 4. Microphotographs of various dislocation patterns indicative of high-temperature plastic deformation in olivine crystals. (a,b) The youngest 1977 picrite lava flow near Piton Sainte Rose; (c) the ~250-ky-old RP02 picrite from the uppermost part of the Rivière des Remparts cliff (small dimension of the photograph ~120 μm); (d) mantled olivine from the 1977 picrite (small dimension ~1 mm).

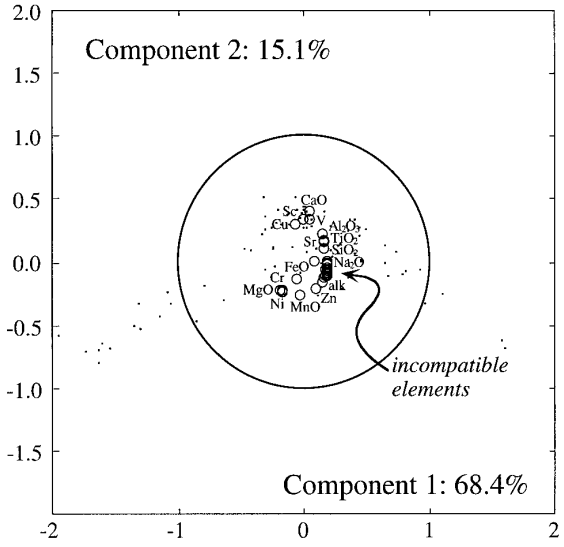

Fig. 6. Principal component analysis of the whole-rock compositions of the four lava series. The unit circle shows the 1σ locus. Two components explain 83·5% of the variance. The samples form an L-shaped array: one arm (left) is made up by the picrites, and the other arm by the mildly alkalic lavas. The common (steady-state) basalts cluster at the apex. ○, projection of the unit vector on each element axis onto the component plane.

observed. The products of Piton de la Fournaise steadily evolved from mildly alkaline to slightly tholeiitic lavas. This is particularly clear in the total alkali vs silica diagram (Fig. 7), where the Remparts series plots well above the discrimination line between alkali basalts and tholeiitic basalts of Macdonald & Katsura (1964). The Nez-de-Boeuf series is still on the alkalic side, whereas the Langevin and the modern series straddle the line, which accounts for the transitional character assigned to the Piton de la Fournaise magmas by the earlier workers (Upton & Wadsworth, 1966, 1972*a*; Ludden, 1978; Nativel *et al.*, 1979). The average extent of differentiation decreases with time, as shown by the decrease of the FeO/MgO ratio (Table 3) whereas the negative correlation of the Al_2O_3/CaO and FeO/MgO ratios (Fig. 8) indicates that clinopyroxene fractionation took a dominant part in producing some of the most differentiated lavas.

Although sampling was not carried out randomly, the histograms of MgO content (Fig. 9a) and alkalinity index (Fig. 9b), defined as $(Na_2O + K_2O) - 0{\cdot}37(SiO_2 - 39)$, show a strong mode with two tails. From ~400 ka to the present, the dominant lavas are basalts with 6–8% MgO and nearly neutral alkalinity with little, though identifiable, chemical variability. These basalts will be subsequently referred to as 'steady-state basalts'. Alkaline lavas form one variant of this well-defined peak with alkalinity indices in excess of +2%. Picritic basalts form a second variant with MgO contents extending from 10 to 27%.

Several major element plots such as FeO–MgO (Fig. 10), CaO– and Na_2O–MgO (Fig. 11a), and Al_2O_3–CaO (Fig. 11b) substantiate and clarify the relationships between these groups. The field of the data reported by Albarède & Tamagnan (1988) for the historical lavas is shown for comparison. Picrites and picritic basalts form a linear array which connects the composition of olivine with 84% forsterite to that of the steady-state basalts. The most magnesian picrite (LGV14) also has a particularly high Al_2O_3/CaO ratio, which indicates some kind of clinopyroxene control. Most alkalic lavas plot off the picritic trend and form a distinct trend pointing away from the clinopyroxene ± plagioclase field. The plagioclase-rich samples (RP18, RP25, RP31, RP32) plot between the field of steady-state basalts and that of plagioclase and indicate plagioclase accumulation.

Trace elements

The compatible transition elements Ni, Cr, Mn and Zn are associated with FeO and MgO in the PCA results (Fig. 6). Ni and Cr show a relationship particularly consistent with those found between major elements (Fig. 12). The steady-state basalts form a linear trend with Ni contents of 60–120 p.p.m. and Cr contents of 50–450 p.p.m. The picritic basalts form a narrow band, possibly regrouping the linear arrays of individual series, at an angle with the trend of steady-state basalts.

The distributions of the rare-earth elements (REE) (Fig. 13) and other incompatible elements resemble what was reported previously by Zielinski (1975), Ludden (1978), Clocchiatti *et al.* (1979) and Albarède & Tamagnan (1988). Amongst the new results, it can be observed that the mild light REE (LREE) enrichment of the least differentiated lavas (La/Yb ~10 ± 2) does not seem to change significantly with time (Table 3). Contrary to concentrations, incompatible element ratios are insensitive to dilution by phenocrysts. To reduce the strong effect of melting, however, the choice of Yb, which is virtually constant in most basaltic liquids (Hofmann & Jochum, 1996), as the normalizing element is preferable to that of a very incompatible element such as Th, Nb or La. The good correlation of Sc/Yb with CaO/Al_2O_3 (Fig. 14) requires that clinopyroxene fractionation has been important at all stages of Fournaise evolution. The Eu anomaly, as measured by the Eu/Eu* ratio, is insignificant or slightly positive, except in the differentiated lavas of the Remparts series, where it may be substantially positive or negative (Fig. 15). Incompatible element concentrations were corrected for the presence of olivine phenocrysts with 83% forsterite assuming olivine–liquid equilibrium (Fig. 16). It was found that, when plotted against CaO as an indicator of clinopyroxene removal, compatibility increases in the order Ce, Yb, Sc. Amongst

Table 3: Mean values of critical concentrations and ratios in the four series investigated in the present study with standard deviation given in parentheses

	Modern	Langevin	Nez-de-Boeuf	Remparts
age (ka)	0	>40	>140	290–530
FeO/MgO	1·09 (0·52)	1·39 (0·52)	1·43 (0·26)	2·30 (0·70)
CaO/Al_2O_3	0·82 (0·07)	0·76 (0·06)	0·66 (0·07)	0·68 (0·10)
MgO (%)	14·26 (3·32)	10·21 (5·61)	8·48 (1·63)	6·44 (3·30)
FeO (%)	12·04 (0·59)	11·67 (0·55)	11·75 (0·45)	12·96 (1·30)
alk (%)	–0·08 (0·48)	0·09 (0·30)	0·70 (0·25)	0·94 (0·62)
Ni (p.p.m.)	453 (154)	271 (291)	178 (77)	96 (150)
Th (p.p.m.)	1·9 (0·6)	2·5 (0·6)	2·8 (0·3)	3·2 (1·2)
Sc (p.p.m.)	26 (1)	28 (4)	25 (4)	28 (7)
Sr (p.p.m.)	277 (69)	356 (68)	400 (39)	437 (59)
Yb (p.p.m.)	1·7 (0·3)	1·9 (0·4)	2·3 (0·2)	2·4 (0·6)
Sc/Th	14·6 (2·4)	11·6 (5·0)	9·1 (1·8)	9·9 (4·0)
La/Yb	9·3 (0·5)	10·4 (1·1)	10·2 (0·8)	10·3 (1·4)
Eu/Eu*	1·02 (0·07)	1·01 (0·04)	1·02 (0·01)	1·17 (0·16)
Th/U	3·6 (0·3)	4·0 (0·8)	4·0 (0·2)	4·3 (1·0)
Nb/La	1·33 (0·03)	1·27 (0·03)	1·32 (0·04)	1·33 (0·06)
Nb/U	41·6 (2·7)	41·8 (7·6)	43·0 (2·1)	44·3 (9·5)
Zr/Nb	7·5 (0·4)	7·5 (0·4)	7·7 (0·5)	7·1 (0·5)

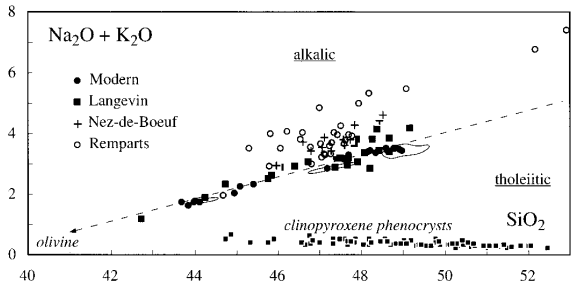

Fig. 7. Total alkali vs silica plot for the Piton de la Fournaise lavas. The tholeiitic/alkalic critical line corresponds to a control by olivine with ~80% forsterite. Clinopyroxene control is the major cause for basaltic compositions to move across the critical line (O'Hara, 1968). The open fields enclose the historic lavas (Albarède & Tamagnan, 1988). The critical line is from Macdonald & Katsura (1964).

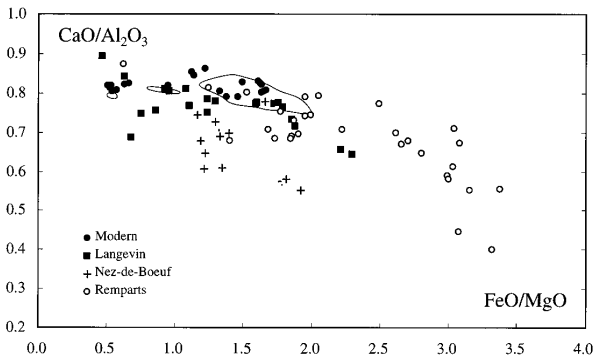

Fig. 8. Correlation between the FeO/MgO and Al_2O_3/CaO ratios revealing extensive removal of clinopyroxene.

the elements that seem to be compatible with clinopyroxene, Sc, V and, to a lesser extent, Cu correlate significantly with CaO.

The Nb/La ratio is fairly constant ($1{\cdot}30 \pm 0{\cdot}03$) but higher than the chondritic value of 1·04 (Sun & McDonough, 1989). Another constant, non-chondritic ratio is the Nb/U ratio ($42{\cdot}9 \pm 1{\cdot}3$). The Th/U ratio is particularly high and changes from 3·6 in modern lavas to 4·0 in the Langevin and Nez-de-Boeuf series and 4·3 in the Remparts series (Fig. 17). These values are in agreement with the range reported by Zielinski (1975), Nativel *et al.* (1979), Deniel *et al.* (1989) and Deniel (1990), but are significantly higher than the value of 3·0 observed for the modern Hawaiian volcanoes (Hofmann & Jochum, 1996). Groundwater circulation may have leached U from old samples. The Cs content varies in a fairly systematic way up the stratigraphic column but, except

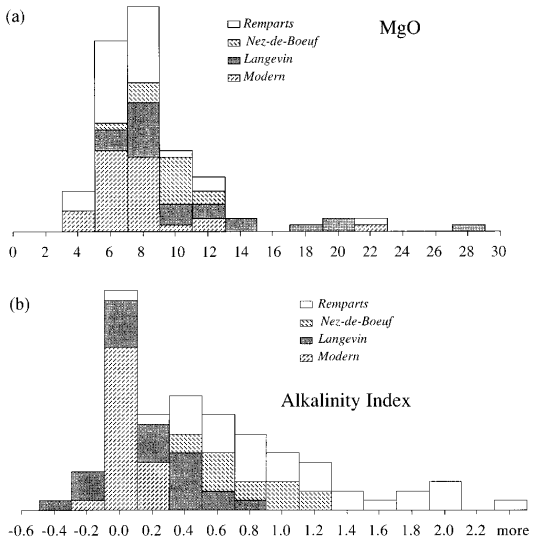

Fig. 9. (a) Histogram of the MgO contents in the analysed samples from the Piton de la Fournaise. The high-MgO samples (picrites) form a tail distinct from the main peak of the steady-state basalts and differentiated lavas. (b) Histogram of the alkalinity index (in per cent excess $Na_2O + K_2O$) in the samples from Piton de la Fournaise. The lavas from the Remparts series are clearly more alkalic and form a tail with respect to the peak of 'steady-state' transitional basalts. The smallest rectangles correspond to one measurement.

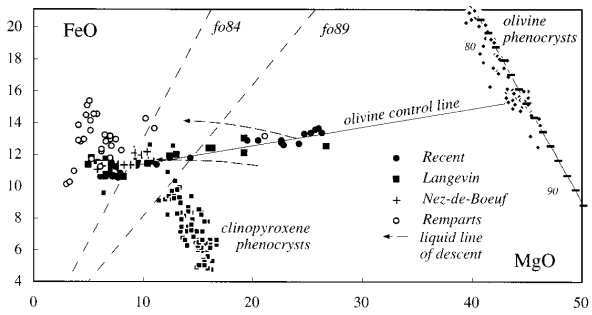

Fig. 10. Plot of FeO and MgO contents of the whole-rock, olivine and clinopyroxene samples. A liquid in equilibrium with fo_{XX}, XX being the forsterite content, should plot at the intersection of the fo_{XX} dashed line and of the corresponding olivine control line. The observed olivine control line shows that the picrites correspond to the entrainment of olivine with ~83% forsterite by a basalt nearly identical to the steady-state basalts. For reference, two liquid lines of descent with olivine removal (arrows) have been calculated using the algebraic solution of Albarède (1992). The dashed lines are the loci of liquids in equilibrium with olivine Fo_{84} and Fo_{89} assuming 13% Fe in ferric state. The Remparts series shows a pronounced Fe enrichment attributable to clinopyroxene removal.

for the most differentiated and the picritic lavas, its systematics seem to have been controlled by mobility rather than magmatic processes.

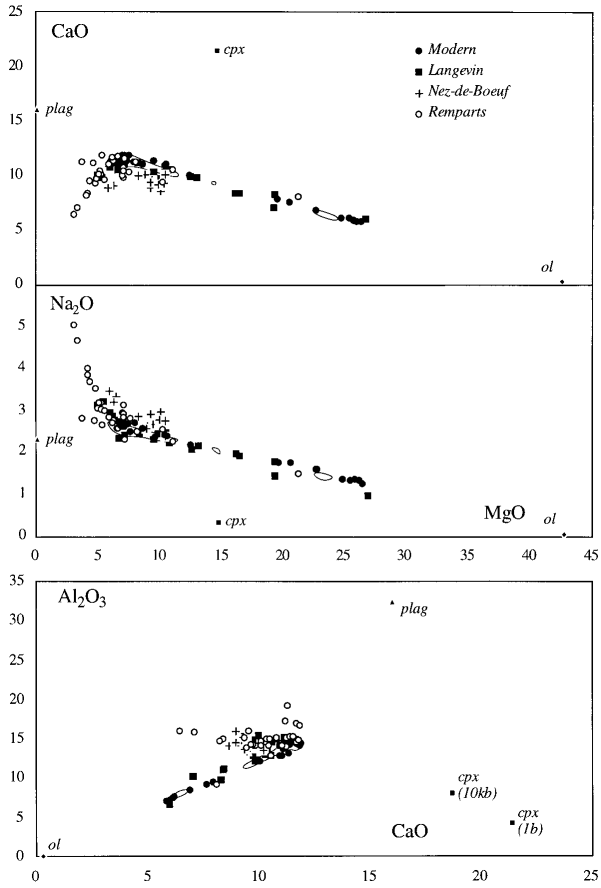

Fig. 11. Plot of the CaO, Na_2O, Al_2O_3 and MgO contents of the whole-rock, olivine, and clinopyroxene samples showing the olivine control line and the prominent effect of clinopyroxene removal in the Remparts and Nez-de-Boeuf series. (Note the excess Al_2O_3 in the four plagioclase-phyric samples RP18, RP25, RP31, and RP32, which indicates that gabbroic cumulates have been entrained by these lavas.) 'cpx (1b)' stands for the average clinopyroxene phenocryst composition, 'cpx (10kb)' for the clinopyroxene composition in the experiments of H. Mesnil & M. Baker (personal communication, 1996).

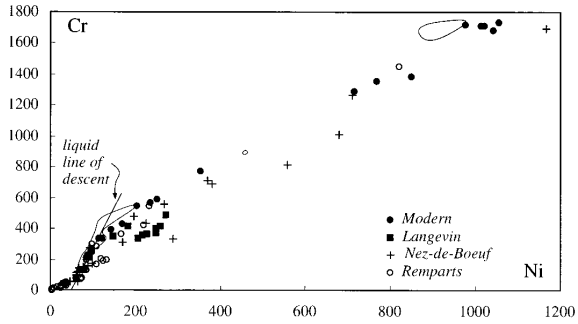

Fig. 12. The contents of Cr and Ni in the whole-rock samples. The open field is that of the historic lavas (Albarède & Tamagnan, 1988). The liquid line of descent in basalts makes an angle with the picritic array which indicates that these two features are not related to one another in the same fractional crystallization process.

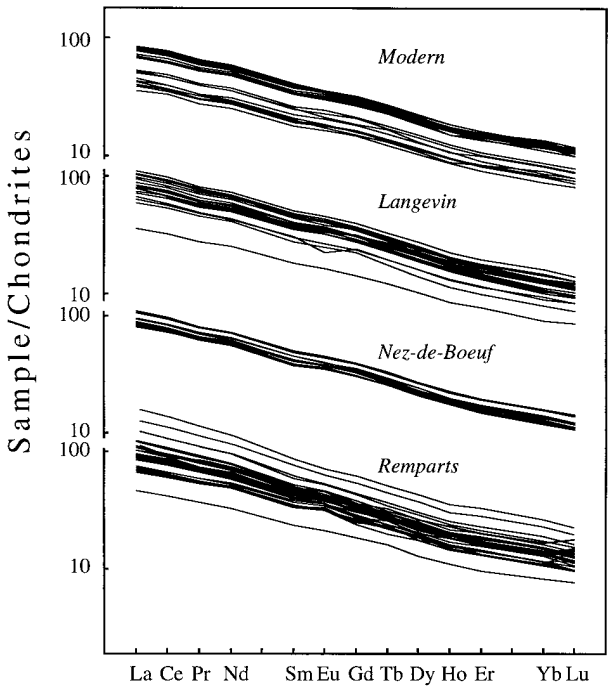

Fig. 13. Rare-earth element concentrations in the whole-rock samples in a chondrite-normalized plot.

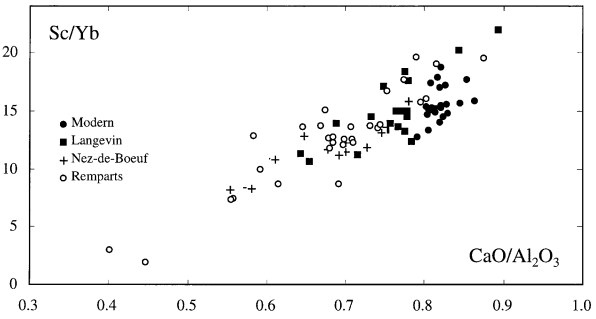

Fig. 14. Plot of the Sc/Yb and CaO/Al_2O_3 ratios in each series. The good correlation emphasizes a control by clinopyroxene which removes Sc and Ca preferentially to Yb and Al.

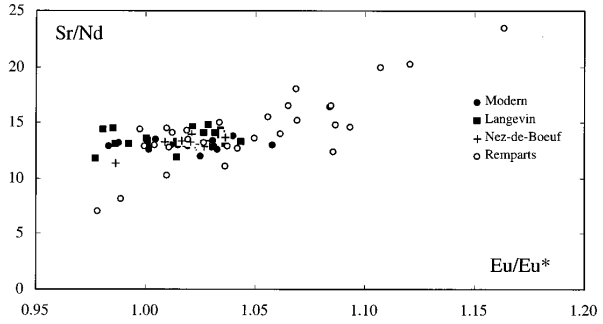

Fig. 15. Plot of Eu/Eu* vs Sr/Nd which suggests that the Eu anomaly observed in the Remparts series results from plagioclase accumulation and removal.

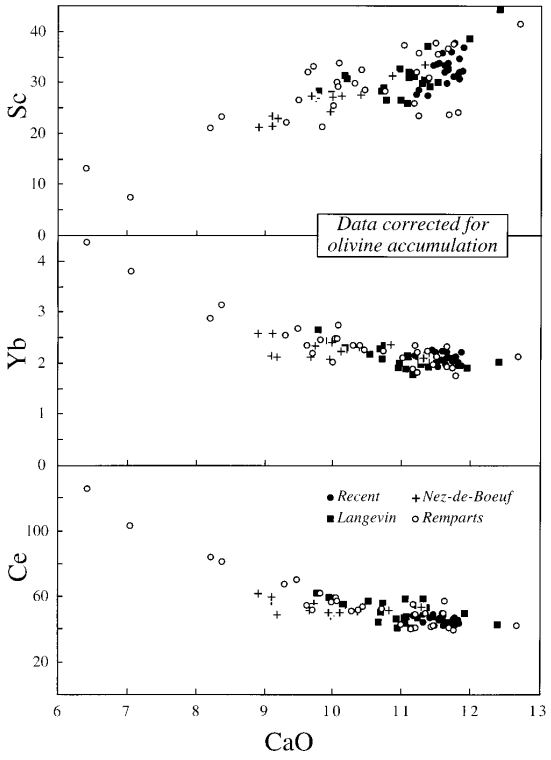

Fig. 16. Plot of olivine-accumulation corrected concentrations of Sc, Yb and Ce vs CaO. Olivine is assumed to contain 83% forsterite and $K_D = 0{\cdot}30$. Compatibility increases in the order Ce, Yb, Sc, which indicates clinopyroxene control.

Sr isotopes

The overall variations of the $^{87}Sr/^{86}Sr$ ratio over 530 ky is small (0·70403–0·70425) and in the range of the values reported by Fisk *et al.* (1988). When the picrites, which seem to contain Sr more radiogenic than the basalts and differentiated products, are excluded, $^{87}Sr/^{86}Sr$ correlates significantly neither with FeO/MgO (Fig. 18) nor with the alkalinity index. Stratigraphic plots show no long-term correlation between $^{87}Sr/^{86}Sr$ and incompatible element ratios such as La/Yb.

MAGMA DIFFERENTIATION

Olivine–liquid relationships

None of the lavas can be considered as representing a primary magma extracted from a peridotitic source. The olivine basalt samples are clearly too poor in MgO, Ni and Cr to be in equilibrium with mantle peridotite. For reasons that will appear later, we believe that we cannot calculate a precise liquid line of descent. In addition,

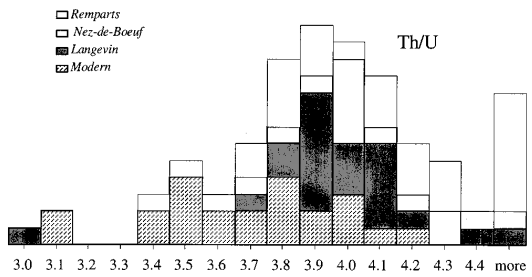

Fig. 17. Histogram of Th/U ratios in the four investigated series of lavas. The mean ratio decreases with time.

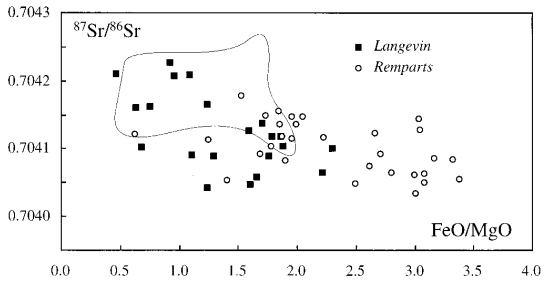

Fig. 18. Plot of $^{87}Sr/^{86}Sr$ vs FeO/MgO. Comparison of the new data with the field drawn with the data of Albarède & Tamagnan (1988) should be made with caution. Picrites seem to have slightly more radiogenic Sr, which is interpreted as reflecting assimilation of hydrothermally altered cumulates.

three arguments indicate that picritic basalts do not represent primary melts:

(1) Their FeO/MgO ratio is too low to record equilibrium with mantle peridotite (>90% forsterite).

(2) The presence of dislocations in some large olivine crystals (Fig. 4a–c) indicates high-temperature plastic deformation that cannot be acquired in a melt (Nicolas & Poirier, 1976; Boudier, 1991). The mantled olivines (Fig. 4d) also show the presence of xenocrystic cores. As stated in a previous section, some lavas contain abundant ultramafic inclusions, mostly dunite and wehrlites, disaggregating into individual olivine crystals.

(3) As discussed by Albarède & Tamagnan (1988), the whole-rock Ni–Cr trend of Fig. 12 in the olivine basalts requires that the cumulate composition lies on the alignment of this trend. For compatible elements, ideal fractional crystallization must produce strongly curved patterns in both the residual liquid and the cumulus phases (e.g. Albarède, 1995). The linear array of the picritic basalts is therefore a mixing line. The sharp angle between this trend and the olivine basalt trend indicates that the picrites and picritic basalts have incorporated olivine crystals that cannot be the unmodified mineral extracts from the basalt sequence. The FeO–MgO plot of Fig. 10 also indicates a linear mixing trend in the picritic basalts at an angle with the liquid line of descent. This trend is imperfect because clinopyroxene is entrained together with olivine (see below). The FeO and MgO content of the interstitial melt in equilibrium with picritic olivine crystals with 84% forsterite is found on the mixing line at the point where the K_D of Roeder & Emslie (1970) is equal to 0·3. For 13% ferric iron in the liquid, it is found that the interstitial liquid contains ~8·3% MgO and 11·4% FeO_T and is therefore only slightly more primitive than the steady-state basalts.

The persistence of dislocations in olivine xenocrysts may seem inconsistent with the overall Fe–Mg equilibrium partitioning illustrated in Fig. 10 and their rather high CaO content. Sobolev & Nikogosian (1994) estimated that, regardless of the composition of the source, the primary Réunion basalts formed at a temperature >1380°C. Using the data of Jurewicz & Watson (1988*b*) on Fe–Mg–Ca diffusion in olivine, it is found that 1-mm sized olivine crystals equilibrate with basaltic liquid at a lower temperature of 1300°C in <10 yr. Chemical equilibrium is therefore achieved rather fast, well before all dislocations become fully annealed. Kink-bands have actually been observed in olivine crystals from the Kilauea Iki lava lake 22 yr after the eruption (Helz, 1987). Nevertheless, the origin of olivine xenocrysts does not seem to reside in mantle peridotites. The persistence of devitrified glass inclusions and the similarity of Cr-spinel inclusions in deformed and non-deformed olivine crystals together with the lack of mantle-derived xenoliths contrasting with abundant olivine-rich cumulate inclusions (Babkine *et al.*, 1966; Upton & Wadsworth, 1972*b*) strongly indicate that the olivine xenocrysts derive from the mechanical disaggregation of earlier cumulates (Albarède & Tamagnan, 1988). Olivines with kink-bands, likewise indicative of plastic deformation, have been observed in the olivine-rich lavas of Kilauea (Helz, 1987; Clague *et al.*, 1995) and Mauna Kea (Yang *et al.*, 1994; Garcia, 1996; Baker *et al.*, 1996). Kink-bands normally form upon migration of dislocations during thermal restoration at high temperature and their presence attests to a particularly strong deformation regime (Nicolas & Poirier, 1976). Dislocation-bearing olivine crystals that are only mildly deformed or remain at high temperature only for a short time are therefore not expected to show kink-bands and may normally be mistaken as undeformed phenocrysts grown from the surrounding melt. Few of the Piton de la Fournaise olivine crystals observed to contain dislocations actually show well-developed kink-bands or undulose extinction. The abundance of olivine crystals with kink-bands in a particular range of forsterite content (Clague *et al.*, 1995; Garcia, 1996; Baker *et al.*, 1996) is therefore not a reliable measure of the extent of cumulate cannibalism nor is their absence a criterion of the unfractionated character of picritic lavas.

Fractionation of the differentiated lavas

Calcium concentrations in lavas lower than, or equal to, those of a primary melt from the mantle (Hirose & Kushiro, 1993; Baker *et al.*, 1995) and correlated variations of FeO/MgO and CaO/Al_2O_3 (Albarède & Tamagnan, 1988, and Fig. 8) visible in all the Piton de la Fournaise products indicate pyroxene control. Most samples from the lower alkalic part of the Remparts series form a trend from olivine basalt to hawaiite and mugearite compositions. The least differentiated basaltic lavas are slightly more alkaline than the modern olivine basalts but there is a considerable overlap of all the series in a range of composition that we identified as the 'steady-state basalt' composition. For all lavas, some olivine fractionation is required to account for the low Ni contents, the spread in SiO_2 (Fig. 7), and the rather high FeO/MgO ratios of the lavas. As shown, however, by the whole-rock FeO/MgO and CaO/Al_2O_3 ratios and by the Fe^{2+}, Ti and Al contents of clinopyroxene phenocrysts, fractionation in the Remparts series was dominated by this mineral. Accumulation–fractionation-corrected Sc concentrations decreasing by a factor of three from the basalts to the mugearites (Fig. 16) and values of partition coefficients such as those suggested by Hart & Dunn (1993) and Green (1994) require that clinopyroxene is the major mineral constituent of the cumulate. This observation is similar to that made on Kohala by Hofmann *et al.* (1987). Such a strong clinopyroxene control is also required by the correlation of the CaO/Al_2O_3 ratio with the Sc/Yb ratio (Fig. 14) and by the position of the whole-rock Remparts trend in several plots, such as CaO vs MgO, CaO vs Al_2O_3 and FeO vs MgO, with respect to the composition of each mineral (Figs 10 and 11). The composition of the cumulate removed by ideal fractionation from the melt cannot be assessed with precision by, for example, least-squares, as the plagioclase/clinopyroxene ratio seems to increase when differentiation proceeds. This is particularly visible in the Na_2O–MgO plot of Fig. 11a. The presence of even small fractions of cumulative or xenocrystic plagioclase confers on the rock a positive Eu anomaly that overwhelms the negative anomaly produced by mineral fractionation (Fig. 15) and therefore limits the value of this element as an indicator of plagioclase removal. Nearly constant Sr concentrations in the most differentiated lavas and the correlated variations of Sr/Nd with Eu/Eu*, however, suggest that the cumulates contained 20–30% plagioclase. Examination of Fig. 11 (a and b) shows that olivine was not an important constituent ($\leq 10\%$). From the enrichment factor (~3) estimated for the Ce concentrations after correction for olivine accumulation–fractionation (Fig. 16), we suggest that the differentiated lavas formed from the basalts by removal of 0–70% of a gabbroic cumulate constituted of 20–40% plagioclase, 70–30% clinopyroxene and $\leq 10\%$ olivine.

The high-precision isotope dilution data of Albarède & Tamagnan (1988) on historical steady-state basalts show a good correlation between Ce/Yb and CaO/Al_2O_3 which the precision of the present data set allows to be seen on the most differentiated data only. The consistent variations of the FeO/MgO and CaO/Al_2O_3 ratios (Fig. 8) therefore suggest that some ratios of incompatible elements may be affected by the fractionation of a relatively high-pressure mineral assemblage with abundant clinopyroxene. For further use in the section dealing with depth of fractionation, the proportion of clinopyroxene actually present in the plagioclase-free cumulate of the steady-state basalts with 'normal' Eu/Eu* and Sr/Nd ratios (Fig. 15), should be evaluated. During fractional crystallization, the Sc/Yb ratio in the residual liquid varies according to the Rayleigh law and F, the fraction of residual liquid, can be estimated as

$$F=\left[\frac{(\mathrm{Sc/Yb})_{\mathrm{residue}}}{(\mathrm{Sc/Yb})_{\mathrm{parent}}}\right]^{\frac{1}{D_{\mathrm{Sc}}-D_{\mathrm{Yb}}}}.$$

Let us conservatively assume that the bulk cumulate-liquid partition coefficients D obey $D_{\mathrm{Yb}} \ll D_{\mathrm{Sc}}$ and adopt Hart & Dunn's (1973) value of 1·3 for the partition coefficient of Sc between clinopyroxene and basaltic liquid, with olivine and all other mineral phases being devoid of this element. Changing the Sc/Yb ratio by a factor of two, which is a reasonable range for all the series investigated (Fig. 14), can be achieved through the precipitation of 65% of a wehrlite cumulate with equal proportions of olivine and clinopyroxene. The same effect on the Sc/Yb ratio is obtained by precipitating 41% of monomineralic clinopyroxenite. Piton de la Fournaise lavas therefore must have fractionated substantial amounts of clinopyroxene.

The origin of alkalinity

The three prehistoric series (Remparts, Nez-de-Boeuf and Langevin) include lavas that are on the alkalic side of the discrimination line of Macdonald & Katsura (1964). The mean composition of the Piton de la Fournaise products clearly becomes less alkalic with time (Table 3). Changes are more noticeable in the upper part of the Remparts cliff but a clear alkalic 'flavour' is still perceived in the Nez-de-Boeuf series (Fig. 7), which is ~350 ky younger than the oldest Piton de la Fournaise lava flows. The transition from alkali basalts to tholeiites deduced from the compounded underwater observations collected during several dives on the northeastern flank of the Loihi seamount by Garcia *et al.* (1995) seems to occur faster than at Piton de la Fournaise.

The strong negative correlation of the alkalinity index with the CaO/Al_2O_3 ratio (see Fig. 20, below) supports

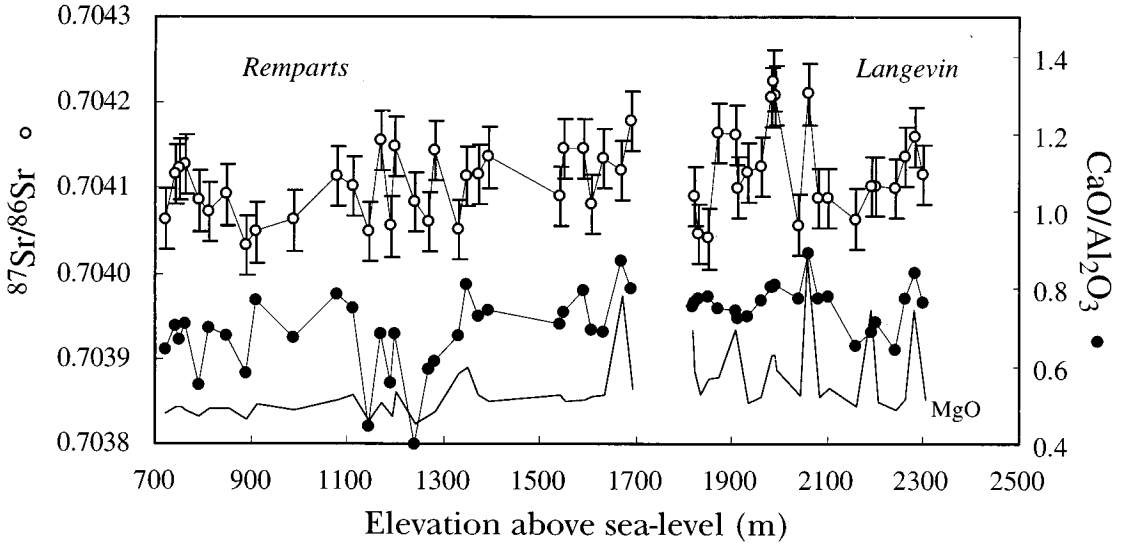

Fig. 19. Plot of $^{87}Sr/^{86}Sr$ (○) vs stratigraphic position. The CaO/Al_2O_3 ratio (●, right axis) and MgO contents (line without symbols, no scale) are shown for comparison. Most picrites from the Langevin series have more radiogenic Sr.

the original suggestion of O'Hara (1968) that the lavas become alkalic upon massive removal of clinopyroxene. Although the role of clinopyroxene fractionation in the differentiation of alkali basalts was repeatedly noticed (Feigenson *et al.*, 1983; Duda & Schmincke, 1985; Frey *et al.*, 1990), the difference between alkali and tholeiitic basalts is usually ascribed to isotopically different sources (Chen & Frey, 1983). In the case of Piton de la Fournaise, the lack of correlation between alkalinity and the $^{87}Sr/^{86}Sr$ ratios (Fig. 19b) in non-picritic basalts suggests that the dominant control of alkalinity is not the source composition. The discrimination line in Macdonald & Katsura's (1964) alkalinity–silica diagram (Fig. 7) was drawn in such a way that the alkalinity index of basalts is left unaltered by fractionation or accumulation of olivine containing ~80% forsterite. In contrast, substantial clinopyroxene removal drives basalts from the tholeiitic into the alkalic field. The alkalic and tholeiitic basalts from Piton de la Fournaise may have a common source and the same parent magma but their fractionation history has been extremely different.

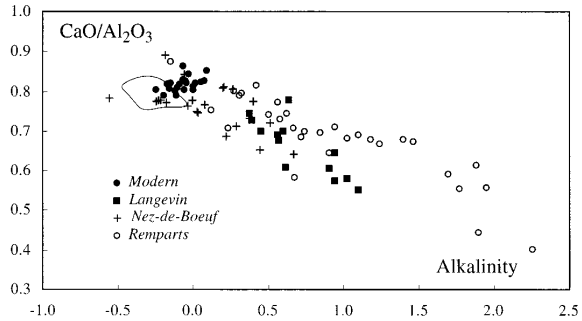

Fig. 20. The good correlation between the CaO/Al_2O_3 ratio and the alkalinity index indicates that clinopyroxene fractionation creates alkalinity in many Piton de la Fournaise lavas. This observation substantiates a model first expressed by O'Hara (1968).

Depth of fractionation

The main features of olivine tholeiite fractionation were long ago established experimentally by Green & Ringwood (1967). The more recent experimental results of Mahood & Baker (1986) on Pantelleria basalts, and of Fisk *et al.* (1988) on Piton de la Fournaise, complemented by unpublished experiments by H. Mesnil & M. Baker (personal communication, 1996), refine the model of Green & Ringwood with only slight differences. Figure 21 summarizes with some accuracy the phase relationships of a basalt similar to what we defined as a steady-state basalt. Olivine is the liquidus phase up to 8 kbar and does not seem to reach saturation at any temperature near the liquidus at deeper levels. The cross-over with clinopyroxene as the liquidus phase occurs at 9 ± 2 kbar. Green & Ringwood (1967) mentioned that orthopyroxene joins clinopyroxene upon cooling at high pressure. Plagioclase crystallizes before pyroxene at low pressure and after pyroxene at high pressure down to at least 10 kbar. The clinopyroxene–plagioclase cross-over is located at 4 ± 1 kbar.

Albarède & Tamagnan (1988) found that the phenocrysts from the historical basalts of the Piton de la

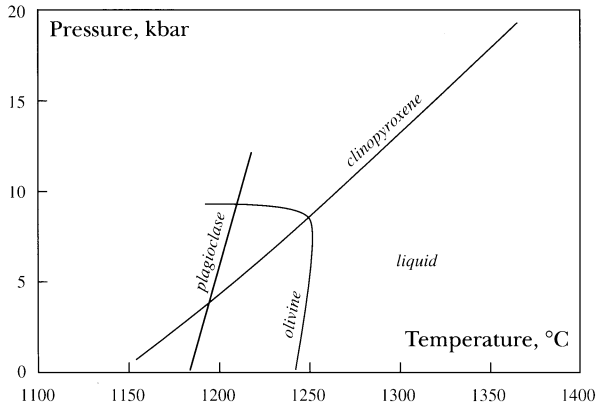

Fig. 21. Tentative saturation boundaries of olivine, clinopyroxene and plagioclase in Piton de la Fournaise basalts near steady-state composition from the experimental work of Fisk *et al.* (1988), Green & Ringwood (1967), and H. Mesnil & M. Baker (personal communication, 1996). The pyroxene–plagioclase cross-over is at 4 ± 1 kbar, the clinopyroxene–olivine cross-over at 9 ± 2 kbar.

Fournaise crystallize in the order olivine–clinopyroxene–plagioclase, i.e. in the same sequence as noted by Upton & Wadsworth (1972*b*) in the Piton de Chisny cumulate xenoliths. These observations place fractionation at >4 kbar, i.e. at depth exceeding those of geophysical anomalies which could be interpreted as reflecting a stagnant magma chamber (Lénat & Aubert, 1982). The presence of plutonic rocks at relatively shallow depth under the volcano (Rançon *et al.*, 1989) requires that magmas have occasionally been trapped in sills and dykes, not the presence of a long-standing magma chamber capable of feeding long sequences of volcanic eruptions. Polybaric fractionation of a clinopyroxene-rich, olivine-poor gabbroic assemblage at moderate pressure (~8–10 kbar), and of olivine at higher levels (4–8 kbar) seems to be prevalent. In general, a significant trend towards less fractionation and decreasing clinopyroxene/olivine ratio in the cumulate of younger rocks is visible in the mean values of the alkalinity index (Figs 7 and 9b; Table 3), and of the range of CaO/Al_2O_3 and Sc/Yb ratios (Fig. 14). This trend indicates that differentiation takes place at increasingly higher levels with time. Subdued but perfectly identifiable clinopyroxene removal associated with incompatible element fractionation ([Albarède & Tamagnan (1988) and above] suggests that, however dominated by low-pressure olivine control, the historical lavas still go through some clinopyroxene fractionation. This fractionation pattern casts some doubt on the validity of trace element modelling aimed at describing the distribution of melts and the residual mineralogy in the mantle source when the geochemical variability is limited (Hofmann & Feigenson, 1983; Albarède & Tamagnan, 1988; McKenzie & O'Nions, 1991).

The presence of clinopyroxene-rich cumulates should be visible as a velocity increase in seismic profiles across hotspots. The high velocity observed at depth >15 km at the base of the crust and in the lithosphere under the Marquesas (Caress *et al.*, 1995) and Réunion (Driad *et al.*, 1995) could indicate the abundance of these cumulates. A petrological model to account for that correspondence has been proposed by Farnetani *et al.* (1996).

Buffered differentiation in an ascending slurry-zone

The apparently innocuous observation that the Piton de la Fournaise lavas can be divided into a dominant type (the 'steady-state basalts') and two subordinate series with fairly variable compositional patterns poses the more difficult question of the relationships between the geochemical diversity of the lavas and the differentiation mechanism. A similar situation was addressed by Rhodes (1988) for Mauna Loa, for which most bulk compositions are 'perched' at the intersection of an olivine control line with a trend for more differentiated lavas. Let us first investigate the compositional variability produced by mineral fractionation. The differential form of the Rayleigh equation can be written for an element subscripted i as

$$\frac{\mathrm{d}C_i}{C_i} = (D_i - 1)\frac{\mathrm{d}f}{F} \cdot$$

This equation is of little interest for incompatible elements whose variations should be dominated by fluctuations, however small, of the melting regime. For compatible elements, however, the dispersion $\mathrm{d}C_i/C_i$ of the concentrations of very compatible elements in residual melts varies rapidly with the fraction of crystals removed. Conversely, this equation can be used to estimate $\mathrm{d}F/F$ from the dispersion $\mathrm{d}C_i/C_i$ of a compatible element i when its solid–liquid fractionation can be estimated. For basalts with 4% < MgO < 9% (which includes most of the aphyric steady-state basalts in the histogram of Fig. 9a), a relative dispersion (standard deviation divided by mean value) of $\pm 18\%$ is observed for MgO and $\pm 54\%$ for Ni. For pure olivine fractionation, the mineral data and experiments suggest $D_{MgO} \sim 5{\cdot}5$, $D_{Ni} \sim 18$. The relationship above would require a relative dispersion of the fractionation extent of only $18/4{\cdot}5 = 4\%$ and $54/17{\cdot}0 \sim 3\%$, respectively. Chromium shows the same pattern but dealing with Cr fractionation by chromite is confusing. These values are surprisingly small and consistent. Buoyancy-driven eruption is probably not an effective mechanism to bring differentiation to a halt at a fixed MgO content: Piton de la Fournaise lavas with olivine phenocryst contents varying from 0 to 50% have widely different densities but seem to be emitted equally easily. A density minimum, which Sparks *et al.* (1980) and Stolper & Walker (1980) assumed to reduce the

compositional spread of ocean- floor tholeiites and layered intrusions, is unlikely to occur in the steady-state basalts, which lack significant plagioclase fractionation. An alternative mechanism is needed that allows the Piton de la Fournaise to erupt substantially differentiated lavas for which the differentiation extent is nearly constant over several hundred thousand years.

Rhodes (1988) explained the surprisingly narrow variability of most Mauna Loa lavas by a regime of continuously erupting and replenished magma chamber (O'Hara, 1977). Physically, however, the compatible element variability has the same origin for both closed and open regimes to the point that for a steady-state magma chamber the formal expression of variability is identical. An open magma chamber underlying the volcanoes does not therefore explain a small range of compatible element concentrations.

Buffering compatible elements in the steady-state basalts requires that the liquids equilibrated with their cumulate assemblages in a solid-dominated environment, a situation much reminiscent of the melting conditions. The FeO/MgO ratio and the Ni concentration of the basalts indicate that the dominant solid phase cannot be mantle material. This suggests that, just before eruption, the steady-state basalts must have equilibrated with an olivine $\pm$ clinopyroxene assemblage which imposes its compatible element characteristics on the interstitial magmatic liquid. This condition can be achieved in a number of ways such as successive equilibration between melt and crystals at different levels, but percolation of liquids through a crystal slurry is certainly an efficient process. Unless a dyke is wide (>2 m), its blocking by crystallization occurs in a matter of days (Bruce & Huppert, 1990). It is therefore intuitive that magmas rise more easily through hot pre-existing dykes than through cold lithosphere. We imagine that the plumbing system of the volcano is filled with unconsolidated cumulates from previous eruptions. The secular equilibrium of the ^{238}U–^{228}Ra pair and $^{226}Ra/^{230}Th$ ratios of ~1·3–1·4 have been interpreted by Sigmarsson *et al.* (1995) as indicating that magmas travel for 100–1000 yr from the mantle source to the surface. Alternatively, it may indicate that the lavas contain a melt component that had a long residence time in deep-seated dykes. Solitary porosity waves are known to form in wet porous media and travel unmodified over long distances (Scott & Stevenson, 1984, 1986; Barcilon & Richter, 1986; Olson & Christensen, 1986; Whitehead & Helfrich, 1990). A somewhat analogous process, described as diapiric melt transfer, was described on a small scale in the olivine-rich lavas of the Kilauea Iki lava lake by Helz *et al.* (1989). Because the steady-state lavas appear to be saturated with these phases, the mineral composition of the slurry must be dominated by olivine with ~84% forsterite, spinel and, in proportions decreasing toward the surface, calcic pyroxene. This mineralogy is therefore extremely similar to that of the 'cumulates' from Piton Chisny (Babkine *et al.*, 1966; Upton & Wadsworth, 1972*b*) and to some plutonic rocks from the Grand Brûlé drill hole (Rançon *et al.*, 1989).

Scott & Stevenson (1986) suggested that zone-refining is an appropriate model for the assessment of solid–liquid mass-balance during the passage of a porosity wave. Albarède (1995) adapted Pfann's (1952) equation for zone-refining to the case of a crystal mush (Fig. 22). Whether the solid forms a porous rigid framework or a loose slurry is immaterial to the present mass-balance argument. A packet of magma percolates through the mush, forming a column of solid–liquid suspension of finite height L. In the suspension zone, volume porosity is Φ. When the liquid escapes, it leaves behind a volume porosity φ of trapped melt. The solid–liquid partition coefficient of element i is D_i. The conservation equation and its solution are given in the Appendix. A characteristic distance z_i over which the concentration of element i varies by a factor e is defined as

$$z_i = \frac{\Phi\rho_{liq} + (1-\Phi)\rho_{sol}D_i}{\varphi\rho_{liq} + (1-\varphi)\rho_{sol}D_i} L .$$

The depth of seismicity (a few kilometres) just before eruptions (Bachèlery *et al.*, 1982; Lénat & Aubert, 1982; A. Hirn, personal communication, 1995), combined with the duration (several weeks) and velocity (~1 m/s) of eruptions, suggests that the magma column is at least several kilometres high. Compatible elements, for which $z_i \sim L$, are buffered over a short distance. Their concentration in the interstitial melt is therefore rapidly buffered during the ascent of the magma within the lithosphere. By contrast, for small values of D_i, $z_i \sim \Phi L/(\varphi + D_i) \gg L$. Small fractions φ of trapped liquid therefore increase dramatically the characteristic distance. A solitary wave with $\Phi = 50\%$ liquid, as in the picritic basalts, leaving behind a cumulate with $\varphi = 0{\cdot}5\%$ residual porosity would transport unaffected distributions of very incompatible to moderately incompatible elements ($D_i \ll \varphi$), such as Th, Ba, Sr, Nd and Zr, over distances of ~100L, i.e. across the entire lithosphere. Not unexpectedly, the journey of the melt through the slurry should not visibly perturb its incompatible element distribution.

Unlike fractional crystallization, the slurry-zone model successfully predicts several features of the Piton de la Fournaise lavas:

(1) The small spread of compatible element concentrations in otherwise differentiated basalts.

(2) The lack of mantle xenoliths in basalts owing to the presence of a mineral slurry lid on top of the dyke system. Picrites from Mauna Kea have actually been found to contain small cumulate xenoliths with plastically deformed olivine crystals (Garcia, 1996). This feature was previously interpreted as reflecting the presence

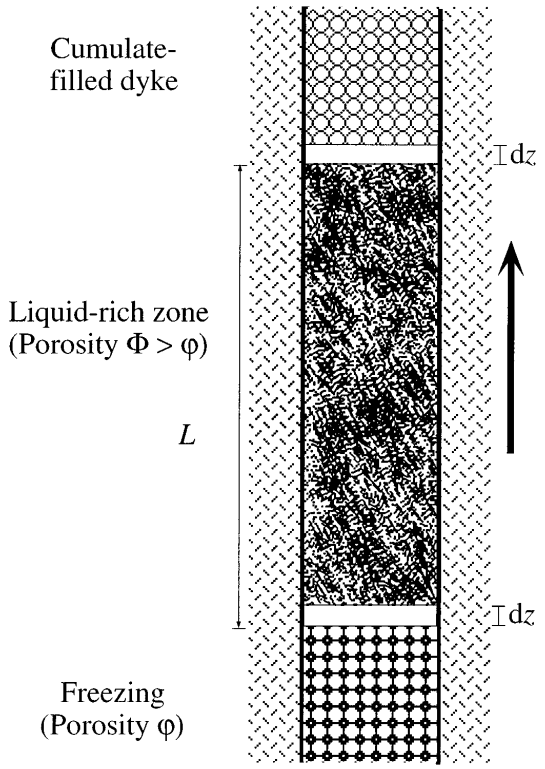

Fig. 22. Layout of the slurry-zone model. A liquid-rich zone with length L and porosity Φ moves upward in a dyke leaving behind a cumulate with residual porosity φ (Albarède, 1995). This zone partial-melting model is in essence a continuous equilibrium crystallization model.

of intermediate to shallow magma reservoirs [see, for instance, the concept of hydraulic filters described by Clague (1987)] which are difficult to reconcile with residence time analysis.

(3) The presence in the picrites of plastically deformed olivines in equilibrium with the interstitial melt. Thin dykes and sills can be severely and repeatedly deformed at high temperature with the slurry they contain provided the fraction of interstitial liquid is small.

(4) The origin of picrites. Abundant olivine crystals can be entrained upon flushing of the conduits during stronger eruptions. Clinopyroxene is probably much less abundant in the slurry from the uppermost levels of the plumbing system. Gravitational settling during the flushing of olivine slurry-filled dykes also explains the greater abundance of olivine in vents near sea-level than in those located at the summit when picritic lava is erupted simultaneously at different elevations (Kieffer *et al.*, 1977).

For incompatible elements, the contribution of the dyke-filling unconsolidated cumulates during the passage of the porosity wave is probably small and, as shown in the Appendix,

$$C^i_{\mathrm{liq}}(z) \sim C^i_{\mathrm{liq}}(0)\exp(-z/z_i).$$

The log–log plots of compatible elements should therefore present linear arrays with slopes different from that characteristic for Rayleigh fractionation. The closed system condition which is the crux of Rayleigh distillation does not hold for the slurry-zone model and, as in the Ni–Cr plot (Fig. 12), the crystal slurry does not necessarily plot as an extension of the liquid array as required by the Rayleigh fractionation law.

A frustrating corollary of the proposed model is that, because the solid–liquid interaction depends on the previous history of the dyke-filling mush, the liquid line of descent of the basalts cannot be rigorously calculated from the mineral equilibrium data and a simple fractionation model. Even a simple model such as that of O'Hara (1968) relating alkali basalts and tholeiites through polybaric fractionation becomes difficult to assess in a cumulus-dominated regime. If the only cumulus minerals were those present in the picrites, we could apply the sketchy equilibrium crystallization 'equation' parent magma → cumulus + residual melt, and retrieve the composition of the parent magma along the olivine control line which would be in equilibrium with highly magnesian olivine (Fig. 10). For 89% forsterite in the olivine (the highest value recorded so far on the volcano), such a primary magma would contain 14·5 wt % MgO, 12·3 wt % FeO, 11·6 wt % Al_2O_3 and 12·0 wt % CaO, a composition up to 1% richer in iron than that estimated by Sobolev & Nikogosian (1994). It can be expected, however, that the bottom of the zone of dykes filled with poorly consolidated cumulates reaches down to levels (~25 km) where clinopyroxene replaces olivine as the liquidus mineral. In this respect, we note that the most magnesian picritic samples, such as LGV14, also have the highest CaO/Al_2O_3 and Sc/Yb ratios, indicating the presence of cumulus clinopyroxene. Experimental petrology provides only loose control on cumulate composition at depth. Surprisingly, compatible elements such as Ca and Cr and, to a lesser extent, Sc, V and Cu should also be buffered at depth by clinopyroxene, although the lavas may show all the signs of an overwhelming olivine control acquired at low pressure.

In contrast to steady-state basalts, the large geochemical variability of the volcanic products from the differentiated Remparts series indicates a liquid-dominated context of fractional crystallization. The existence of large reservoirs of magmatic liquid is unlikely, as they would be unstable at the pressure indicated by the clinopyroxene-dominated liquidus (>8 kbar). Wall differentiation (Irving, 1980; Bruce & Huppert, 1990) in deep dykes pried open through a cold part of the lithosphere reconciles the geochemical variability, the occasionally large extents of differentiation and the mineralogy of the cumulate.

THE GEOCHEMICAL SIGNATURE OF VOLCANIC CANNIBALISM

The presence of plastically deformed olivine crystals, the Mg–Ni–Cr systematics of basalts and picrites reported by Albarède & Tamagnan (1988) and in the present work, and the presence of dismantled gabbroic fragments in the differentiated lavas of the Remparts series (RP18, RP25, RP31, RP32) indicate that cannibalization of earlier crystallization products is a common phenomenon. Such a process may be suspected to bias the trace element and isotopic signature of the lavas with respect to that of primary basalts with major consequences. In particular, the transfer times derived from U–Th series disequilibria may prove difficult to interpret if melt trapped in residual porosity is allowed to interact with fresh batches of magma.

More importantly, the very existence of an olivine control line indicates that the interstitial melt in picrites consists of steady-state basalt. The slightly higher $^{87}Sr/^{86}Sr$ ratio in the picrites with respect to other lavas at comparable $^{143}Nd/^{144}Nd$ ratios (this work and B. Luais, unpublished results, 1996) therefore signals that the disaggregated products may have interacted with seawater to some extent through deep hydrothermal circulation around magmatic conduits filled with slurry. Plutonic material with indications of intense hydrothermal alteration was actually described in the cuttings of the Grand Brulé drill hole (Augé *et al.*, 1989; Lerebour *et al.*, 1989; Rançon *et al.*, 1989).

Hauri *et al.* (1996) reported a good correlation between Mg, Ni and Cr in the Mauna Kea olivine basalts, which indicates that a large fraction of the Os isotopic signal in these rocks must be associated with the presence of olivine crystals, which those workers viewed as essentially cognate minerals. Hauri *et al.* (1996) and Eiler *et al.* (1996) concluded that the isotope systematics of Os, Sr, Nd, Pb and O rule out the involvement of the lithosphere in the formation of Hawaiian shield basalts. If, however, some Fournaise basalts are capable of disaggregating up to 1/1 proportions of olivine-rich cumulates and, as in Hawaii, partially redissolve the xenocrysts (Helz, 1987; Garcia, 1996), it is likely that they can simultaneously assimilate other rocks, especially those with a low melting point, such as altered basalts from the volcanic edifice and its underlying oceanic crust. Contamination at relatively shallow level of picrites with a high content of xenocrystic olivines still needs full consideration.

TRANSIENT AND STEADY-STATE MELT EXTRACTION

The preceding discussion has suggested that the early history of Piton de la Fournaise, a volcano widely recognized as producing transitional basalts, is actually dominated by a fractionation scheme typical of alkalic lavas. The transition from tholeiitic to alkalic lavas has been thoroughly investigated in Hawaii (Macdonald & Katsura, 1964; Feigenson *et al.*, 1983; Frey *et al.*, 1990, 1991; Chen *et al.*, 1991), and to a much lesser extent, for Piton des Neiges (Upton & Wadsworth, 1972*a*; Ludden, 1978; Rocher, 1990). The early stages of a shield volcano and particularly the relations of early alkalic rocks to the shield lavas are less well known for three possible reasons: (1) scarcity of relevant field data as in the case of the Loihi seamount (Frey & Clague, 1983; Garcia *et al.*, 1995); (2) blanketing of the early rocks by young lava flows combined with subsidence; (3) the early alkalic stage is not as common as speculated.

For Piton de la Fournaise, the K–Ar data indicate that differentiated lavas belonging to an alkalic trend were erupted between ~530 and 400 ka. The first steady-state basalts and picrites appear in the last quarter of the Remparts series, presumably ~350 ka ago. Although some later progressive changes in the differentiation processes are observed, this transition is certainly a major event in the evolution of the volcanic system. The early period was characterized by deeper differentiation, and therefore more efficient cooling upon ascent, and large chemical variability. These two features may be ascribed to small magma input rates in narrow transient conduits. In contrast, the steady-state basalts represent residual liquids of buffered low-pressure fractionation, which indicates that the input rate was large, thereby reducing heat loss and crystal fractionation. These contrasting features agree with the standard view of volcanic regimes such as that of Clague (1987). They can alternatively be viewed as the contrasting transient and steady-state regimes of magma extraction at the top of the hotspot conduit.

We suggest that the early alkalic stage samples the thermal boundary layer of the conduit whereas the steady-state basalts and picritic surges are extracted from the hot core with minimum thermal variability. Interestingly, the duration of the waning alkalic stage of Piton des Neiges is comparable [190–60 ka according to Rocher (1990)] with that of the early alkalic stage of Piton de la Fournaise (530–350 ka), and the shield stages of the two volcanoes do not seem to overlap. Using the plate velocity of 0·15 deg/my estimated by Gripp & Gordon (1990), the Indian plate moved by ~3 km during the early alkalic stage of Piton de la Fournaise and the waning alkalic stage of Piton des Neiges. In contrast, the plate moved by ~6 km since the first recorded eruption of the Fournaise steady-state basalts. In comparison, the known 2 my lifetime of Piton des Neiges corresponds to a displacement of the plate of 33 km.

These distances may be related in different ways to hotspot dynamics (Frey & Rhodes, 1993). First, the plate

can be assumed to move above a long cylindrical hotspot conduit. The more alkalic lavas tap the rim of the cylinder whereas the tholeiitic lavas represent melts from the core. The radius estimated by fluid mechanics for plume conduits is actually well within the range of the observed displacements: for steady pipe flow, Loper & Stacey (1983) quoted a range of 10–12 km, whereas Whitehead & Helfrich (1990) estimated a radius of 14 km for waves in conduit (pulsated transport). Réunion, however, sits on top of an almost perfectly conical bathymetric bulge and geoid, separated from the bulge around Mauritius by a pronounced bathymetric low (Bonneville *et al.*, 1988). A model of a steady cylindrical hotspot conduit does not explain these features, nor how the hotspot activity jumps from Piton des Neiges to Piton de la Fournaise in a direction perpendicular to the hotspot track. Alternatively, the hotspot activity may be viewed as a string of solitary waves (blobs) of material with excess potential temperature, each wave being associated with the growth of an individual volcano. Beneath the lithosphere, both the front and the tail of each hot solitary wave produce less melt that evolves as mildly alkalic lavas when it burns through the cold lithosphere. In contrast, the hotter main body produces melts which keep their tholeiitic affinity on their way through a heated lithosphere. The ascent velocity of the mantle material can be computed as the ratio of the volume flux of hotspot material to an estimated area of the hotspot horizontal cross-section. Sleep (1990) [see also Davies (1988)] related the nose of the bathymetric high to a stagnation curve and used the volume of the swell in a fluid mechanic model to estimate the material flux under the Réunion hotspot as 85 m^3/s. A cylindrical hotspot with a radius of 200 km would require that hot mantle material moves upwards at 2 cm/yr whereas a smaller hotspot with a radius of 50 km would rise at 34 cm/yr. If, in addition, the height of the cylinder is assumed to equal the ascent velocity times 2·1 my and is equal to the diameter of the blob, we obtain a preferred radius of 100 km and an ascent velocity of 9 cm/yr. This calculation is reasonably robust with respect to the lifetime of the volcano. If it is 5 my instead of 2·1 my, a radius of 130 km and an ascent velocity of 5 cm/yr are obtained. Numerical experiments indeed suggest that the ascent velocity of a solitary wave may be somewhere in that range (Scott & Stevenson, 1986).

CONCLUSIONS

(1) The character of differentiation at Piton de la Fournaise changes from mildly alkalic to mildly tholeiitic over the known lifetime of the volcano (530 ky).

(2) Clinopyroxene fractionation drives tholeiitic basalts into the field of alkali basalts.

(3) Mineral fractionation becomes shallower with time as olivine replaces clinopyroxene as the liquidus phase.

(4) Modelling of the melting process should take high-pressure fractional crystallization into account.

(5) Plastically deformed phenocrysts are observed. Cumulate cannibalism should affect the geochemical properties of the lavas.

(6) The buffering of the compatible element compositions is inconsistent with magma chamber processes. It is thought to result from the ascent of melt-rich zones through dykes filled with a slurry of olivine $\pm$ clinopyroxene.

(7) Picrites (= oceanites) form upon flushing the slurry from the dykes.

(8) The more alkalic lavas correspond to a process of dynamic crystallization of a gabbroic assemblage on dyke walls.

(9) This volcano may have formed by the impingement on the base of the lithosphere of a solitary wave of hotspot material with a radius of ~100 km rising with a velocity of 5–9 cm/yr.

ACKNOWLEDGEMENTS

Institut des Sciences de l'Univers under the initiative of Guy J. Aubert and Ministère de l'Education Nationale, both through the programme 'Risques Naturels', made the initial funds available that allowed this work to be realized, notably in the field, through Grants 92 40 01, 93 31 01 and 94 31 07. The European programme on Volcans Laboratoires encouraged collaboration between several research groups and provided most of the funds used for the analyses through Grant EVSV-CT92-0189. Jacques Bertola and Christian Germanaz, at considerable personal risk, carried heavy material down breathtaking cliffs and provided us with unique and fascinating core samples. Jean-Marie Lavèvre, the skilled helicopter pilot, carried out difficult and dangerous tasks. We thank all the colleagues and friends who gave us a hand in the field: Philippe Mairine, André Legros, Jean-Paul Toutain, Annick Chauvin and Yves Gallet. We appreciated the help in the laboratory of Janne Blichert-Toft, Teddy Para, Liliane Savoyant, Simone Pourtalès, Dodie James, Attila Nagy and Françoise Vidal. Considering her incredible talents in solving all the many non-scientific problems, Catherine Netter should have been given a chance to also run the science. Reviews by Al Hofmann, Martial Caroff, Fred Frey and Mike Garcia gave us a chance to correct some misunderstandings. Discussions with Françoise Boudier, Dave Clague, Michel Condomines, Fred Frey, Mike Garcia, Pierre-Yves Gillot, Al Hofmann, Jean-François Lénat, Mike Rhodes, Olgeir Sigmarsson and Bill White have illuminated different points met in this work. Hughes Mesnil and Mike Baker

shared information on their experimental work on the steady-state basalt composition. Annick Chauvin donated her core samples from the Nez-de-Bœuf series.

REFERENCES

Albarède, F., 1992. How deep do common basalts form and differentiate? *Journal of Geophysical Research* **97,** 10997–11009.

Albarède, F., 1993. Residence time analysis of geochemical fluctuations in volcanic series. *Geochimica et Cosmochimica Acta* **57,** 615–621.

Albarède, F., 1995. *Introduction to Geochemical Modeling.* Cambridge: Cambridge University Press.

Albarède, F., 1996. High-resolution geochemical stratigraphy of Mauna Kea flows from the Hawaii Scientific Drilling Project core. *Journal of Geophysical Research* **101,** 11841–11853.

Albarède, F. & Tamagnan, V., 1988. Modelling the recent geochemical evolution of the Piton de la Fournaise volcano, Réunion island, 1931–1986. *Journal of Petrology* **29,** 997–1030.

Augé, T., Lerebour, P. & Rançon, J.-P., 1989. The Grand Brûlé exploration drilling: new data on the deep framework of the Piton de la Fournaise volcano. Part 3: Mineral chemistry of the cumulate rocks. *Journal of Volcanology and Geothermal Research* **36,** 139–151.

Babkine, J., Conquéré, F. & Vilminot, J.-C., 1966. Nodules de péridotites et cumulats d'olivine. *Bulletin de la Société Française de Minéralogie et Cristallographie* **89,** 262–268.

Bachèlery, P. & Mairine, P., 1990. Evolution volcano-structurale du Piton de la Fournaise, depuis 0·53 Ma. In: Lénat, J.-F. (ed.) *Le Volcanisme de la Réunion.* Clermont-Ferrand: Centre de Recherches Volcanologiques, pp. 213–242.

Bachèlery, P., Blum, P.A., Cheminée, J.-L., Chevallier, L., Gaulon, R., Girardin, N., Jaupart, C., Lalanne, F.-X., Le Mouël, J. L., Ruegg, J.-C. & Vincent, P., 1982. Eruption at Piton de la Fournaise volcano on 3 February 1981. *Nature* **297**, 395–397.

Baker, M. B., Hirschmann, M. M., Ghiorso, M. S. & Stolper, E. M., 1995. Composition of low-degree partial melts of peridotite: results from experiments and thermodynamic calculations. *Nature* **375,** 308–311.

Baker, M. B., Alves, S. & Stolper, E. M., 1996. Petrography and petrology of the Hawaiian Scientific Drilling Project samples. *Journal of Geophysical Research*, **101**, 11715–11727.

Barcilon, V. & Richter, F. M., 1986. Non-linear waves in compacting media. *Journal of Fluid Mechanics* **164,** 429–448.

Birck, J.-L. & Allègre, C. J., 1978. Chronology and chemical history of the parent body of basaltic achondrites studied by the ^{87}Rb–^{87}Sr method. *Earth and Planetary Science Letters* **39,** 37–51.

Bonneville, A., Barriot, J. P. & Bayer, R., 1988. Evidence from geoid data of a hotspot origin for the southern Mascarene Plateau and Mascarene Islands (Indian Ocean). *Journal of Geophysical Research* **93,** 4199–4212.

Boudier F., 1991. Olivine xenocrysts in picritic magmas. An experimental and microstructural study. *Contributions to Mineralogy and Petrology* **109,** 114–123.

Bruce, P. M. & Huppert, H. E., 1990. Solidification and melting along dykes by the laminar flow of basaltic magmas. In: Ryan, M. P. (ed.) *Magma Transport and Storage.* New York: John Wiley, pp. 87–101.

Caress, D. V., McNutt, M. K., Detrick, R. S. & Mutter, J. C., 1995. Seismic imaging of hot-spot related crustal underplating beneath the Marquesas Islands. *Nature* **373,** 600–603.

Chen, C.-Y. & Frey, F. A., 1983. Origin of Hawaiian tholeiite and alkalic basalt. *Nature* **203,** 785–789.

Chen, C. Y., Frey, F. A., Garcia, M. O., Dalrymple, G. B. & Hart, S. R., 1991. The tholeiite to alkalic basalt transition at Haleakala Volcano, Maui, Hawaii. *Contributions to Mineralogy and Petrology* **106,** 183–200.

Clague, D. A., 1987. Hawaiian xenolith population, magma supply rates, and development of magma chambers. *Bulletin of Volcanology* **49,** 577–587.

Clague, D. A., Moore, J. G., Dixon, J. E. & Friesen, W. B., 1995. Petrology of submarine lavas from Kilauea's Puna Ridge, Hawaii. *Journal of Petrology* **36,** 299–349.

Clocchiatti, R., Havette, A. & Nativel, P., 1979. Relations pétrogénétiques entre les basaltes transitionnels et les océanites du Piton de la Fournaise (île de la Réunion, océan Indien) à partir de la composition chimique des intrusions vitreuses des olivines et des spinelles. *Bulletin de Minéralogie* **102,** 511–525.

Condomines, M., Hémond, C. & Allègre, C. J., 1988. U–Th–Ra disequilibria and magmatic processes. *Earth and Planetary Science Letters* **90,** 243–262.

Davies, G. F., 1988. Ocean bathymetry and mantle convection 1. Large-scale flow and hotspots. *Journal of Geophysical Research* **93,** 10467–10480.

Deniel, C., 1990. Le magmatisme du Piton des Neiges. In: Lénat, J.-F. (ed.) *Le Volcanisme de la Réunion.* Clermont-Ferrand: Centre de Recherches Volcanologiques, pp. 115–143.

Deniel, C., Condomines, M., Kieffer, G., Bachèlery, P. & Harmon, R. S., 1989. U–Th–Ra radioactive disequilibrium and Sr, O isotopes in Piton des Neiges and Piton de la Fournaise lavas (Réunion Island). In: *IAVCE Conference on Continental Magmatism, 131.* Santa Fe, NM: New Mexico Bureau of Mines and Mineral Resources, p. 72.

Driad, L., Hirn, A., Nercessian, A., Charvis, P., Laesanpura, A. & Gallart, J., 1995. Crustal and upper mantle structure under the Réunion hotspot from seismic and wide angle data. *EOS* **76,** 587.

Duda, A. & Schmincke, H.-U., 1985. Polybaric differentiation of alkalic basaltic magmas: evidence from green-core clinopyroxenes (Eifel, F.R.G.). *Contributions to Mineralogy and Petrology* **91,** 340–353.

Duncan, R. A., Backman, J. & Peterson, L., 1989. Réunion hot spot activity through Tertiary time: initial results of the Ocean Drilling Program, Leg 115. *Journal of Volcanology and Geothermal Research* **36,** 183–198.

Eiler, J. M., Valley, J. W. & Stolper, E. M., 1996. Oxygen isotope ratios in olivine from the Hawaii Scientific Drilling Project. *Journal of Geophysical Research* **101,** 11807–11813.

Farnetani, C. G., Richards, M. A. & Ghiorso, M. S., 1996. Petrological models of magma evolution and deep crustal structure beneath hotspots and flood basalt provinces. *Earth and Planetary Science Letters*, **139**, 333.

Feigenson, M. D., Hofmann, A. W. & Spera, F. J., 1983. Case studies on the origin of basalt II. The transition from tholeiitic to alkalic volcanism on Kohala volcano, Hawaii. *Contributions to Mineralogy and Petrology* **84,** 390–405.

Fisk, M. R., Upton, B. G. J., Ford, C. E. & White, W. M., 1988. Geochemical and experimental study of the genesis of Reunion Island, Indian Ocean. *Journal of Geophysical Research* **93,** 4933–4950.

Fitton, G., Saunders, A. D., Larsen, L. M., Hadarson, B. S. & Norry, M. J., 1996. Volcanic rocks from the southeast Greenland margin at 63°N: composition, petrogenesis and mantle sources. In: Saunders, A. D., Larsen, H. C. & Clift, P. D. (ed.) *Proceedings of the Ocean Drilling Program, Scientific Results*. College Station, TX: Ocean Drilling Progam, in press.

Frey, F. A. & Clague, D. A., 1983. Geochemistry of diverse basalt types from Loihi Seamount, Hawaii: petrogenetic implications. *Earth and Planetary Science Letters* **66,** 337–355.

Frey, F. A. & Rhodes, J. M., 1993. Intershield geochemical differences among Hawaiian volcanoes: implications for source compositions,

melting processes and magma ascent paths. *Philosophical Transactions of the Royal Society of London, Series A* **342,** 121–136.

Frey, F. A., Wise, W. S., Garcia, M. O., West, H., Kwon, S.-T. & Kennedy, A., 1990. Evolution of Mauna Kea volcano, Hawaii: petrologic and geochemical constraints on post-shield volcanism. *Journal of Geophysical Research* **95,** 1271–1300.

Frey, F. A., Garcia, M. O., Wise, W. S., Kennedy, A., Gurriet, P. & Albarède, F., 1991. The evolution of Mauna Kea volcano, Hawaii: petrogenesis of tholeiitic and alkali basalts. *Journal of Geophysical Research* **96,** 14347–14375.

Garcia, M. C., 1996. Petrography and olivine and glass chemistry of lavas from the Hawaii Scientific Drilling Project. *Journal of Geophysical Research* **101,** 11701–11713.

Garcia, M. O., Foss, D. J. P., West, H. B. & Mahoney, J. J., 1995. Geochemical and isotopic evolution of Loihi volcano, Hawaii. *Journal of Petrology* **36,** 1647–1674.

Gillot, P.-Y., Nativel, P. & Condomines, M., 1990. Evolution volcano-structurale du Piton de la Fournaise, depuis 0·53 Ma. In: Lénat, J.-F. (ed.) *Le Volcanisme de la Réunion*. Clermont-Ferrand: Centre de Recherches Volcanologiques, pp. 243–256.

Graham, D., Lupton, J., Albarède, F. & Condomines, M., 1990. A 360,000 year helium isotope record from Piton de la Fournaise, Réunion Island. *Nature* **347,** 545–548.

Green, D. H. & Ringwood, A. E., 1967. The genesis of basaltic magmas. *Contributions to Mineralogy and Petrology* **15,** 103–190.

Green, T. H., 1994. Experimental studies of trace-element partitioning applicable to igneous petrogenesis—Sedona 16 years later. *Chemical Geology* **117,** 1–36.

Gripp, A. E. & Gordon, R. G., 1990. Current plate velocities relative to the hotspots incorporating the NUVEL-1 global plate motion model. *Geophysical Research Letters* **17,** 1109–1112.

Hart, S. R. & Dunn, T., 1993. Experimental clinopyroxene/melt partitioning of 24 trace elements. *Contributions to Mineralogy and Petrology* **113,** 1–8.

Hauri, E., Lassiter, J. C. & DePaolo, D. J., 1996. Osmium isotope systematics of drilled lavas from Mauna Loa, Hawaii. *Journal of Geophysical Research* **101,** 11793–11806.

Helz, R. T., 1987. Diverse olivine types in lava of the 1959 eruption of Kilauea volcano and their bearing on eruption dynamics. *US Geological Survey Professional Paper* **1350,** 691–722.

Helz, R. T., Kirschenbaum, H. & Marinenko, J. W., 1989. Diapiric transfer of melt in Kilauea Iki lava lake, Hawaii: a quick, efficient process of igneous differentiation. *Geological Society of America Bulletin* **101,** 578–594.

Hirose, K. & Kushiro, I., 1993. Partial melting of dry peridotites at high pressures: determination of compositions of melts segregated from peridotite using aggregates of diamond. *Earth and Planetary Science Letters* **114,** 477–489.

Hofmann, A. W. & Feigenson, M. D., 1983. Case studies on the origin of basalt: I. Theory and reassessment of Grenada basalts. *Contributions to Mineralogy and Petrology* **84,** 382–389.

Hofmann, A. W. & Jochum, K.-P., 1996. Source characteristics derived from very incompatible trace elements in Mauna Loa and Mauna Kea basalts (Hawaiian Scientific Drilling Project). *Journal of Geophysical Research* **101,** 11831–11839.

Hofmann, A. W., Feigenson, M. D. & Raczeck, I., 1987. Kohala revisited. *Contributions to Mineralogy and Petrology* **95,** 114–122.

Horn, I., Foley, S. F., Jackson, S. E. & Jenner, G. A., 1994. Experimentally determined partitioning of high-field strength and selected transition elements between spinel and basaltic melts. *Chemical Geology* **117,** 193–218.

Irving, A. J., 1980. Petrology and geochemistry of composite ultramafic xenoliths in alkalic basalts and implications for magmatic processes within the mantle. *American Journal of Science* **280A,** 389–426.

Johnson, R. A. & Winchern, D. W., 1992. *Applied Multivariate Statistical Analysis*. Englewood Cliffs, NJ: Prentice–Hall.

Jurewicz, A. J. G. & Watson, E. B., 1988*a*. Cations in olivine, Part 1: Calcium partitioning and calcium–magnesium distribution between olivines and coexisting melts, with petrologic applications. *Contributions to Mineralogy and Petrology* **99,** 176–185.

Jurewicz, A. J. G. & Watson, E. B., 1988*b*. Cations in olivine, Part 2: Diffusion in olivine xenocrysts, with application to petrology and mineral physics. *Contributions to Mineralogy and Petrology* **99,** 186–201.

Kieffer, G., 1990. Evolution dynamique et structurale récente ('Phase IV') du Piton des Neiges (Ile de la Réunion, Océan Indien). In: Lénat, J.-F. (ed.) *Le Volcanisme de la Réunion*. Clermont-Ferrand: Centre de Recherches Volcanologiques, pp. 163–185.

Kieffer, G., Tricot, B. & Vincent, P. M., 1977. Une éruption inhabituelle (avril 1977) du Piton de la Fournaise (Ile de la Réunion): ses enseignements volcanologiques et structuraux. *Comptes Rendus Hebdomadaires des Séances de l'Académie des Sciences* **285,** 957–960.

Kohlstedt, D. L., Goetze, C., Durham, W. B. & Vander Sande, J., 1976. New technique for decorating dislocations in olivine. *Science* **191,** 1045–1046.

Lacroix, A., 1936. *Le Volcan actif de l'Ile de la Réunion et ses Produits*. Paris: Gauthier-Villars.

Lénat, J.-F. & Aubert, M., 1982. Structure of Piton de la Fournaise volcano (La Réunion Island, Indian Ocean) from magnetic investigations. An illustration of the analysis of magnetic data in a volcanic area. *Journal of Volcanology and Geothermal Research* **12,** 361–392.

Lénat, J.-F. & Labazuy, P., 1990. Morphologie et structures sous-marines de la Réunion. In: Lénat, J.-F. (ed.) *Le Volcanisme de la Réunion*. Clermont-Ferrand: Centre de Recherches Volcanologiques, pp. 43–74.

Lerebour, P., Rançon, J.-P. & Augé, T., 1989. The Grand Brûlé exploration drilling: new data on the deep framework of the Piton de la Fournaise volcano. Part 2: Secondary minerals. *Journal of Volcanology and Geothermal Research* **36,** 129–137.

Loper, D. E. & Stacey, F. D., 1983. The dynamical and thermal structure of deep mantle plumes. *Physics of the Earth and Planetary Interiors* **33,** 304–317.

Ludden, J. N., 1978. Magmatic evolution of the basaltic shield volcanoes of Réunion island. *Journal of Volcanology and Geothermal Research* **4,** 171–198.

Macdonald, G. A. & Katsura, T., 1964. Chemical composition of Hawaiian lavas. *Journal of Petrology*, **5,** 82–133.

Mahood, G. C. & Baker, D. R., 1986. Experimental constraints on depths of fractionation of mildly alkalic basalts and associated felsic rocks: Pantelleria, Strait of Sicily. *Contributions to Mineralogy and Petrology* **93,** 251–264.

Maurel, C. & Maurel, P., 1982. Etude expérimentale de l'équilibre Fe^{2+}–Fe^{3+} dans les spinelles chromifères et les liquides silicatés basiques. *Comptes Rendus Hebdomadaires des Séances de l'Académie des Sciences* **II-295,** 209–212.

McDougall, I., 1971. The geochronology and evolution of the young volcanic island of Réunion, Indian Ocean. *Geochimica et Cosmochimica Acta* **35,** 261–288.

McDougall, I. & Compston, W., 1965. Strontium isotope composition and potassium–rubidium ratios in some rocks from Réunion and Rodriguez, Indian Ocean. *Nature* **207,** 252–253.

McKenzie, D. & O'Nions, R. K., 1991. Partial melt distributions from inversion of rare earth element concentrations. *Journal of Petrology* **32,** 1021–1091.

Nativel, P., Joron, J.-L. & Treuil, M., 1979. Etude pétrographique et géochimique des volcans de la Réunion. *Bulletin de la Société Géologique de France* **21,** 427–440.

Nicolas, A. & Poirier, J.-P., 1976. *Crystalline Plasticity and Solid State Flow in Metamorphic Rocks*. London: John Wiley.

O'Hara, M. J., 1968. The bearing of phase equilibria studies on synthetic and natural systems on the origin and evolution of basic and ultrabasic rocks. *Earth-Science Reviews* **4,** 69–133.

O'Hara, M. J., 1977. Geochemical evolution during fractional crystallization of a periodically refilled magma chamber. *Nature* **266,** 503–507.

Olson, P. & Christensen, U., 1986. Solitary wave propagation in a fluid conduit within a viscous matrix. *Journal of Geophysical Research* **91,** 6367–6374.

Pfann, W. G., 1952. Principles of zone-melting. *Transactions of AIME* **194,** 747–753.

Rançon, J.-P., Lerebour, P. & Augé, T., 1989. The Grand Brûlé exploration drilling: new data on the deep framework of the Piton de la Fournaise volcano. Part 1: Lithostratigraphic units and volcanostructural interpretation. *Journal of Volcanology and Geothermal Research* **36,** 113–127.

Rhodes, J. M., 1988. Geochemistry of the 1984 Mauna Loa eruption: implications for magma storage and supply. *Journal of Geophysical Research* **93,** 4453–4466.

Rocher, P., 1990. Evolution structurale du massif du Piton des Neiges. In: Lénat, J.-F. (ed.) *Le Volcanisme de la Réunion*. Clermont-Ferrand: Centre de Recherches Volcanologiques, pp. 145–161.

Roeder, P. L. & Emslie, R. F., 1970. Olivine–liquid equilibrium. *Contributions to Mineralogy and Petrology* **29,** 275–289.

Scott, D. R. & Stevenson, D. J., 1984. Magma solitons. *Geophysical Research Letters* **11,** 1161–1164.

Scott, D. R. & Stevenson, D. J., 1986. Magma ascent by porous flow. *Journal of Geophysical Research* **91**, 9283–9296.

Sigmarsson, O., Condomines, M., Jakobsson, S. P. & Bachèlery, P., 1995. Magma residence time in Piton de la Fournaise and Elfell volcanoes (abstr.). *Terra Nova* **7,** 153.

Sleep, N. H., 1990. Hotspots and mantle plumes: some phenomenology. *Journal of Geophysical Research* **95,** 6715–6736.

Sobolev, A. V. & Nikogosian, I. K., 1994. Petrology of long-lived mantle plume magmatism: Hawaii, Pacific, and Reunion island, Indian Ocean. *Petrology* **2,** 111–114.

Sobolev, A., Clocchiatti, R. & Dhamelincourt, P., 1983. Les variations de la température, de la composition du magma et l'estimation de la pression partielle d'eau pendant la cristallisation de l'olivine dans les océanites du Piton de la Fournaise (Réunion, éruption de 1966). *Comptes Rendus Hebdomadaires des Séances de l'Académie des Sciences* **296,** 275–280.

Sparks, R. S. J., Meyer, P. & Sigurdsson, H., 1980. Density variations amongst mid-ocean ridge basalts: implications for magma mixing and the scarcity of primitive lavas. *Earth and Planetary Science Letters* **46,** 419–430.

Stieltjes, L. & Moutou, P., 1989. A statistical and probabilistic study of the historic activity of Piton de la Fournaise, Réunion Island, Indian Ocean. *Journal of Volcanology and Geothermal Research* **36,** 67–86.

Stolper, E. M. & Walker, D., 1980. Melt density and the average composition of basalt. *Contributions to Mineralogy and Petrology* **74,** 7–12.

Strang, G., 1988. *Linear Algebra and its Applications*. New York: Harcourt Brace.

Sun, S.-S. & McDonough, W. F., 1989. Chemical and isotopic systematics of oceanic basalts: implications for mantle composition and processes. In: Saunders, A. D. & Norry, M. J. (eds) *Magmatism in the Ocean Basins. Geological Society of London Special Publication* **42**, 313–345.

Upton, B. G. J. & Wadsworth, W. J., 1966. The basalts of Réunion island, Indian Ocean. *Bulletin of Volcanology* **29,** 7–23.

Upton, B. G. J. & Wadsworth, W. J., 1972*a*. Aspects of magmatic evolution on Réunion island. *Philosophical Transactions of the Royal Society of London Seies A* **271,** 105–130.

Upton, B. G. J. & Wadsworth, W. J., 1972*b*. Peridotitic and gabbroic rocks associated with the shield-forming lavas of Réunion. *Contributions to Mineralogy and Petrology* **35,** 139–158.

Whitehead, J. A. & Helfrich, K. R., 1990. Magma waves and diapiric dynamics. In: Ryan, M.P. (ed.) *Magma Transport and Storage*. New York: John Wiley, pp. 53–76.

Yang, H.-J., Frey, F. A., Garcia, M. O. & Clague, D. A., 1994. Submarine lavas from Mauna Kea volcano, Hawaii: implications for Hawaiian shield stage process. *Journal of Geophysical Research* **99,** 15577–15594.

Zielinski, R. A., 1975. Trace element evaluation of a suite of rocks from Reunion island, Indian Ocean. *Geochimica et Cosmochimica Acta* **39,** 713–734.

APPENDIX

This model describes the displacement of a partially liquid zone of constant length L. Let Φ be the volume fraction of liquid. This zone moves through a medium at concentration $C_0(z)$ and leaves a residuum with a volume fraction φ of liquid which will be referred to as residual porosity. ρ_{sol} and ρ_{liq} are the densities of the solid matrix and melt, respectively. The molten zone is well mixed so the reference level for the liquid and solid concentrations is conveniently taken as z. Φ, φ and the solid–liquid partition coefficient are assumed to be constant. When the molten zone has proceeded over a length z, mass balance requires

$$\mathrm{d}L\left[\Phi\rho_{\mathrm{liq}}C^i_{\mathrm{liq}}+(1-\Phi)\rho_{\mathrm{sol}}C^i_{\mathrm{sol}}\right]$$
$$=\{\rho_{\mathrm{sol}}C^i_0(z+L)-\left[\rho_{\mathrm{liq}}\varphi C^i_{\mathrm{liq}}+\rho_{\mathrm{sol}}(1-\varphi)C^i_{\mathrm{sol}}\right]\}\mathrm{d}z.$$

In the right-hand side braces, the first term corresponds to the amount of element i entering the molten zone, and the last two terms to the amount left behind at z. Assuming solid–liquid equilibrium fractionation

$$C^i_{\mathrm{sol}}=D_iC^i_{\mathrm{liq}}$$

and defining enrichment factors

$$k^L_i=\Phi\rho_{\mathrm{liq}}+(1-\Phi)\rho_{\mathrm{sol}}D_i$$

and

$$k^R_i=\varphi\rho_{\mathrm{liq}}+(1-\varphi)\rho_{\mathrm{sol}}D_i$$

the previous equation is rearranged as

$$\frac{k^L_iL}{k^R_i}\frac{\mathrm{d}C^i_{\mathrm{liq}}}{\mathrm{d}z}+C^i_{\mathrm{liq}}=\frac{\rho_{\mathrm{sol}}}{k^R_i}C^i_0(z+L).$$

For constant C^i_0, this equation is integrated as

$$C^i_{\mathrm{liq}}(z)=C^i_{\mathrm{liq}}(0)\exp(-z/z_i)+\frac{\rho_{\mathrm{sol}}}{k^R_i}C^i_0\left[1-\exp(-z/z_i)\right]$$

(Albarède, 1995) where

$$z_i = (k_i^L / k_i^R) L.$$

For $\varphi = 0$ and $\Phi = 1$, the zone-refining equation of Pfann (1952) is obtained.

If the contribution of the unconsolidated cumulate can be neglected, for example, for incompatible elements, the last term on the right-hand side cancels out and a plot of

$$\ln C^j_{\text{liq}} \text{ vs } \ln C^i_{\text{liq}}$$

would be a linear array with slope s^j_i such as

$$s^j_i \sim \frac{\varphi \rho_{\text{liq}} + (1-\varphi)\rho_{\text{sol}} D_i}{\varphi \rho_{\text{liq}} + (1-\varphi)\rho_{\text{sol}} D_j}.$$